## On the Detection of Cirrus Clouds

from

Satellite Measurements

by

Larry Di Girolamo

A thesis submitted to the

Faculty of Graduate Studies and Research

in partial fulfillment of the requirements for the degree of

MASTER OF SCIENCE

March, 1992

Department of Meteorology

McGill University

Montreal, Quebec, Canada

(c) Larry Di Girolamo 1992

#### **ABSTRACT**

A thorough literature review of cloud algorithm validation strategies is presented, with particular emphasis on the problems of detecting cirrus clouds. To further advance our cirrus detection capabilities, a new cloud detection technique is proposed for the Multi-angle Imaging Spectro-Radiometer (MISR), which is scheduled to be on the first platform of the Earth Observing System. Radiative Transfer simulations have been used to develop a Band-Differenced Angular Signature technique. This new technique takes the difference between two solar spectral reflectances as a function of view angle. The resulting angular signature is used to discriminate between high- and low-level clouds and surface reflectance anomalies. This technique, coupled with a Predetermined Clear Sky Threshold developed in this study for MISR, can detect cirrus clouds of visible optical thickness > 0.5 without any a priori knowledge of atmospheric conditions. Other techniques that can be used with MISR (i.e. stereo) are also discussed.

## RÉSUMÉ

Dans ce mémoire nous effectuons une revue de littérature exhaustive des stratégies de validation des algorithmes d'identification des nuages, en particulier des cirrus. Pour améliorer notre capacité de détection des cirrus, nous proposons ici une nouvelle technique pour le Multi-angle Imaging SpectroRadiometer (MISR) instrument qui devrait faire partie de la première platforme du Earth Observing System. Des simulations numériques de transfert radiatif ont été effectuées pour développer cette technique que nous appelons Signature Angulaire par Bands Différenciées. Cette nouvelle technique utilise la différence entre deux réflectivités spectrales solaires en fonction de l'angle de vision. La signature angulaire résultante est utilisée pour distinguer les nuages de haut altitude, des nuages de basse altitude, ainsi que des anomalies de réflectivité du sol. Cette technique, jumelée à l'utilisation d'un seuil pour Ciel Découvert Prédéterminé et dévelopée dans ce mémoire pour le MISR, peut détecter des nuages cirrus d'épaisseur optique visible > 0.5 sans aucune connaissance préalable des conditions atmosphériques. D'autres techniques (i.e. stéréo) pouvant aussi être utilisées avec le MISR sont présentées.

#### **ACKNOWLEDGEMENTS**

I wish to express my sincere gratitude to my supervisor, Dr. Roger Davies, for his expert guidance and thoughtful advice during the course of this study. This thesis would never have taken its present form had it not been for Dr. Davies' dedication to his students.

I would like to thank Lisa Ramsaran; without her vast knowledge of computer operations, this study would surely have taken much more time to complete.

Thanks are also expressed to Paul Vaillancourt for translating the abstract from English into French, and Manor Lalonde for her grammatical corrections and moral support.

Partial support from the Jet Propulsion Laboratory of the California Institute of Technology under Contract No. 959085 is gratefully acknowledged.

Special thanks go out to my parents for always being there whenever I needed them.

## TABLE OF CONTENTS

LIST OF FIG	GURES		. <b>v</b>
LIST OF TA	BLES.	••••••	. vii
CHAPTER	1	Introduction	. 1
CHAPTER	2	Cirrus Cloud Detection Algorithms: A Review	. 7
	2.1	Cloud Detection Techniques	. 7
	2.2	Validation of Satellite Cloud Detection	
		Algorithms	. 13
	2.2.1	Satellite Cloud Detection Algorithm	
		Intercomparison	. 13
	2.2.2	Validation using GOES Imagery	. 18
	2.2.3	Validation using Cloud Climatologies	. 19
	2.2.4	Validation using Surface Observations	. 22
	2.3	Discussion	. 25
CHAPTER	3	A New Cloud Detection Technique using the	
		Multi-angle Imaging SpectroRadiometer	30
	3.1	The Multi-angle Imaging SpectroRadiometer	30
	3.2	A New Cloud Detection Algorithm	33
	3.2.1	The Atmospheric Model	33
	3.2.2	The Ocean Model	35
	3.2.3	Atmosphere-Ocean Model Coupling and	
		Verification	41
	3.2.4	The Predetermined Clear Sky Threshold	
		Technique	49
	3.2.5	The Band-Differenced Angular Signature	
		Technique	59
	3.3	Discussion	7 1
CHAPTER	4	Summary	76
REFERENC	FS		80

# LIST OF FIGURES

Figure	
3.1	Flat surface depiction for Fresnel's equation applications
3.2	Ocean model depiction for upwelling radiation calculations
3.3	R values for different waters40
3.4	The various pathways followed by radiation contributing to the satellite measured radiance
3.5	LOWTRAN 7 simulations of TOA radiance showing the similarity in angular variation between the 0.86 µm radiance and the broadband (0.2 µm - 4.5 µm) radiance
3.5	Comparison of TOA reflectance pattern over clear sky- ocean of atmosphere-ocean model simulations to Taylor and Stowe (1984)
3.7	LOWTRAN 7 simulations of TOA 0.86 µm radiances 51
3.8 (a)	Comparison of thin cirrus cloud with the predetermined clear sky threshold calculated for the MISR-D camera with a RAZ = 180°
3.8 (b)	Comparison of thin cirrus cloud with the predetermined clear sky threshold calculated for the MISR-B camera with a RAZ = 180°
3.8 (c)	Comparison of thin cirrus cloud with the predetermined clear sky threshold calculated for the

	MISR-D camera with a RAZ = 150°	. 57
3.8 (d)	Comparison of thin cirrus cloud with the	
	predetermined clear sky threshold calculated for the	
	MISR-D camera with a RAZ = $90^{\circ}$	. 58
3.9	Band-Differenced Angular Signatures for a SZA = 60°	
	and a RAZ = 60°/120°	61
3.10	Band-Differenced Angular Signatures for a $SZA = 60^{\circ}$	
	and a RAZ = 60°/120°	. 62
3.11	Band-Differenced Angular Signatures for a SZA = $60^{\circ}$	
	and a RAZ = 0°/180°	. 63
3.12	Band-Differenced Angular Signatures for a SZA = 60°	
	and a RAZ = $0^{\circ}$	64
3.13	Band-Differenced Angular Signatures for a SZA = 0°	. 65
3.14	Band-Differenced Angular Signatures for a SZA = 0°	. 66
3.15	Stereo height resolution vs. correspondence resolution	
	for the nadir camera and one other MISR camera	. 74
3 16	The MISR cloud detection algorithm	75

# LIST OF TABLES

Table		
2.1	Current cloud detection techniques applicable to cirrus clouds	9
2.2	Summary of intercomparison of algorithms recently made with reference to cirrus	14
3.1	MISR Instrument Specifications	32
3.2	A summary of the BDAS results	69

#### CHAPTER 1

#### Introduction

"Who can number the clouds by wisdom?" (Job 38.37). For thousands of years, the answer to this question has gone unchallenged. Only recently have scientists begun to recognize the implications of numbering clouds. The "number of clouds" or, in more scientific terms, cloud fraction plays an important role in modulating the radiation within the Earth's climate system. Their effect in the shortwave is to reflect the available solar radiation back to space, hence increasing the Earth's albedo. In the infrared, clouds reduce the loss of terrestrial radiation to space by decreasing the Earth's brightness temperature. The overall effect of clouds, in the annual global mean, is to cool the climate system (Ramanathan et al., 1989). These clouds, however, may be strongly influential on a changing climate system, although it is still unclear what magnitude or even what sign this influence will take (Arking, 1991). The cloud influence depends on cloud type, with marine stratocumulus and cirrus clouds recognized as having the largest effects on the global climate system (Cox et al., 1987). Thus, accurate cloud detection techniques are imperative if we are to further our understanding of clouds in climate. This study will focus on the accurate determination of cirrus cloud amount.

The role of clouds in climate and the importance of obtaining cloud cover climatologies have been stressed by the World Climate Research Program (WCRP) with the launch of the International Satellite Cloud

Climatology Project (ISCCP) which has been obtaining satellite observations of cloud cover since July 1983 (Schiffer and Rossow, 1983). Accurate global cloud cover climatologies are required for both climate monitoring and modelling. Accurate cloud cover monitoring may give an indication of climate change by observing changes in climatological cloudiness. For example, Robinson et ai. (1986) reported that increased cloud cover in polar regions is associated with ice breakup and as a result increased open waters. This may warm polar regions and most likely cause an increase in cloudiness; if this is so, clouds have a positive feedback role on warming polar regions.

In terms of climate modelling, accurate cloud cover climatologies are essential for the success of forming clouds in weather and climate models (e.g. Hansen et al., 1983; Cess, 1987). However, as pointed out by Arakawa (1975), cloud cover alone has little relevance in modelling clouds. Global cloud climatologies need to include the seasonal and geographical distributions of not only cloud amount but cloud type. These are needed to verify and tune the cloud model. For example, general circulation models (GCMs) have been an important tool in forecasting the effects of global warming. Their treatment of clouds, however, has been crude. For example, Cess et al. (1990) reported the effects of cloud feedback of 19 GCMs, ranging from modest negative feedback to strong positive feedback. This large uncertainty indicates that improved cloud parameterization schemes are required.

One of the most eluding clouds in terms of cloud-climate feedback are cirrus clouds. For many years it has been believed that cirrus clouds have a cooling or heating effect at the Earth's surface, depending on

their optical properties (e.g. Manabe and Wetherald, 1967; Cox, 1971). Thin cirrus clouds would enhance the greenhouse effect because their increased infrared emission to the surface outweighs the reduction of solar radiation caused by cirrus cloud-top reflection. The effect is inverted for thicker cirrus clouds. Recently, however, Stephens et al. (1990) reported that these results were influenced by inadequate treatment of the physics of cirrus clouds in the models and that the effects of cirrus cloud feedback on climate still remain unknown. This is due to our limited understanding of the relationships between the size and shape of ice crystals and the gross radiative properties of cirrus.

It has also been recognized that the dynamical aspects of cirrus clouds play an important role in terms of cloud feedback on climate. Ramanathan and Collins (1991) demonstrated the effects of feedback between convection, greenhouse effect, and cirrus clouds may limit the temperatures of tropical waters to less than 305 K. The argument, as concluded from observations of the 1987 El Niño, was that warm oceans produced high thin cirrus which enhanced the greenhouse effect. Large-scale convergence of moisture into the warm oceanic regions, brought about by large-scale circulation systems, also amplifies the greenhouse effect. The process continues to produce cirrus clouds until they become thick enough to reflect the amount of solar radiation needed to arrest further warming. However, in light of the results of Stephens et al. (1990) discussed above, more information must be acquired before any assessment of the role cirrus clouds have on climate feedback can be ascertained.

One of the major problems in acquiring reliable cirrus cloud information is their high altitude, residing as they do in the upper troposphere and lower stratosphere. This makes in situ measurements difficult to obtain. Satellite detection of cirrus clouds, especially thin cirrus clouds, remains difficult for many cloud retrieval algorithms because of the low optical thickness and variable emissivities these clouds possess. Lidar has also been used to detect cirrus clouds (Liou, 1986). Although they are extremely sensitive in detecting cirrus, lidars are inappropriate for obtaining global cloud climatologies because of their scarce global coverage and very small spot size. Also, as reported by Bosenberg et al. (1990) during the International Cirrus Experiment (ICE) (Raschke et al., 1989), remote sensing using lidar has many limitations in real eving accurate microphysical quantities of cirrus clouds. Another program designed to examine the microphysical, as well as the macrophysical and radiative properties of cirrus clouds is the First ISCCP Regional Experiment (FIRE) (Cox et al., 1987). FIRE has brought together a multitude of observational techniques to study cirrus, including measurements from satellite, aircraft, surface, and weather balloons. Ultimately the efforts of such experiments as FIRE and ICE will lead to an improved understanding of the physical processes that govern cirrus clouds and the subsequent parameterization of these processes in General Circulation Models.

Satellite observations still remain the most practical method of obtaining cirrus cloud properties at many spatial and temporal resolutions. Many cloud retrieval algorithms exist which use satellite data to determine cloud properties, but there is no single technique that is capable of

coping with the many different cloud and surface type scenarios for accurate cloud detection. The algorithms which focus on particular cloud and surface types are generally superior to those which try to encompass global detection of all cloud types over all surface types. Cloud algorithms all comprise two basic steps: cloud detection and cloud analysis (Rossow et al., 1985). The first step separates the observed radiances into either a clear or cloudy category. The methodology used in the separation determines the type of cloud retrieval algorithm. The second step concerns the quantitative determination of cloud properties derived from the observed cloudy radiances. This may be as simple as summing up the cloudy pixels to obtain cloud fraction, or as complex as fitting the observed cloudy radiances to radiative transfer model outputs to obtain parameterized cloud properties. A major effort of ISCCP war to stimulate research and development of cloud algorithms in order to choose the most appropriate algorithm to analyze the ISCCP data. This has prompted many efforts in validating cloud algorithms; the major limitation is the lack of a "truth" data set against which to compare results (Rossow et al., 1985). The importance of obtaining accurate cirrus cloud properties, particularly cirrus cloud fraction and cirrus cloudtop height, is noted as ISCCP's highest science priority (Schiffer and Rossow, 1983).

In an ongoing effort to meet the science requirements of ISCCP, this study focuses on cirrus cloud detection from satellite remote sensing. Chapter 2 reviews recent (post 1987) accomplishments in cloud detection techniques, which offer the capability of detecting cirrus clouds. This includes not only new algorithms but also older algorithms in which fur-

ther validation, either by intercomparison between other algorithms or via surface observations, has been done. Since the importance of accurate cirrus cloud cover climatology has been stressed, Chapter 2 also focuses on the accuracy of various cloud detection techniques. In order to further our capabilities in cirrus detection, Chapter 3 develops a new technique for the upcoming Multi-angle Imaging SpectroRadiometer which will be launched on the first platform of the Earth Observing System (NASA, 1991). Finally, Chapter 4 summarizes the findings of this study.

#### **CHAPTER 2**

#### Cirrus Cloud Detection Algorithms: A Review

#### 2.1 Cloud Detection Techniques:

Traditionally, cloud detection techniques have been divided into three classes: radiance threshold techniques, radiative transfer model techniques, and statistical techniques (Rossow et al., 1985; Goodman and Henderson-Sellers, 1988). In essence, however, all have some defined threshold, in the sense that a value of a selected quantity divides the population of the measured quantity into either clear or cloudy sections. A review of these cloud detection classes is not presented here as this has been done fairly recently (Rossow, 1989; Goodman and Henderson-Sellers, 1988; Rossow et al., 1985). Instead, the following paragraph gives a brief description.

Briefly then, radiance threshold techniques treat each image pixel separately. Single channel, multi-channel, or some difference of channel-measured radiances are compared to a value of that quantity which divides clear and cloudy pixels (the threshold). The threshold may be selected in a number of ways; these may include a spatial or time series analysis over the region being analyzed and choosing one of the extrema in radiance as clear sky, or using model calculations of the clear sky value (Rossow, 1989). Once the quantity defining clear sky is determined, the threshold value is set above the uncertainty level in the measured clear sky quantity. Radiative transfer model techniques use one or more spectral radiance measurements as input to an atmospheric radiative transfer model

and converts them into some physical quantity. These physical quantities (such as optical thickness and/or cloud-top altitude) are then judged to be clear or cloudy (e.g. from Rossow et al., 1989: visible optical thickness > 1.2; cloud-top altitude > 1.4 km). Statistical techniques use a large group of pixels in a scene all at once. The spectral signature, or some variance thereof, of each image pixel is projected into a multi-dimensional radiance space forming a multi-dimensional histogram in which areas of large pixel density exist. These areas may represent not only different cloud types but also different clear sky surfaces, such as land vs. ocean. Partitions (thresholds) are set up on the histogram which divide each class.

Many cloud algorithms exist which use satellite measurements (e.g. Rossow et al., 1989); however, each algorithm is designed for a particular data set with a particular task in mind. Thus, cloud algorithms normally cannot be used interchangeably. Table 2.1 lists the cloud detection techniques that have been developed since 1987, and have been used in detecting cirrus clouds. Almost all use at least one infrared spectral channel. This is because of the infrared spectrum's dominance in detecting middle and high clouds as compared to the visible regime (Seze and Desbois, 1987; Parker and Wielicki, 1989). Generally these algorithms can be divided into four classes.

The first uses the IR radiance in the classic threshold sense. Here, under the assumption that the brightness temperature of the cloud is colder than the underlying surface and that the cloud emissivity is equal to one, the IR radiance is converted to an equivalent brightness temperature. If the retrieved brightness temperature is less than the clear sky

Table 2.1. Current cloud detection techniques applicable to cirrus clouds.

Method	Reference
	1101010100
Dynamic IR threshold	Coakley (1987)
	Inoue (1987)
Functional box counting	Lovejoy et al. (1987)
Hybrid bispectral threshold method (HBTM)	
Bispectral (multiparameter) threshold (improved cluster technique)	`
IR temperature sounding (improved from Susskind <i>et al.</i> , 1984)	
IR spectral discrimination and threshold (simulation)	
IR spectral discrimination and threshold	Yamanouchi et al. (1987)
VIS threshold and spatial coherence method	
IR spectral discrimination	Prabhakara <i>et al.</i> (1988)
VIS spectral discrimination	Sakellariou and Leighton (1988)
Multispectral retrieval using a variety of methods	Saunders and Kriebel (1988)
IR spectral discrimination	Smith et al. (1988)
IR threshold with clear sky data and UV radiance (NCLE)	
Hybrid histogram-spatial coherence method (adapted from Liu et al., 1988)	
Minimum residual method using sounder data (simulation; adapted from Susskind et al., 1987)	
Bispectral threshold radiative transfer model	` '
Bispectral threshold: Maximum Likelihood Estimator (adapted from Smith <i>et al.</i> , 1986)	Wielicki and Green (1989)
Multispectral discrimination and threshold	Allen et al. (1990)
Local dynamic threshold and non-linear Rayleigh model	
NCLE (Stowe <i>et al.</i> , 1988) using a variable threshold	Eck and Kalb (1991)

<sup>&</sup>lt;sup>a</sup>Spectral discrimination techniques use two or more spectral channels and their differing wavelength dependences to identify clear vs. cloudy conditions.

brightness temperature by a certain amount (the threshold), then the area is labeled as cloudy. The brightness temperature is then compared to the vertical temperature profile to classify the cloud by height (low, middle, and high are the typical divisions). As will be discussed later, cirrus clouds are often misclassified as low or middle clouds because they often have emissivities less than one. Cloud detection is also very sensitive to the clear sky threshold; thus, the methods differ in the way the threshold is chosen (i.e. Coakley, 1987; Stowe et al., 1988; Rossow et al., 1989) and applied in concert with other spectral channels and techniques (i.e. Minnis et al., 1987; Seze and Desbois, 1987, Rossow et al., 1989).

A second class makes use of local spatial variance of the radiance field (e.g. Seze and Desbois, 1987; Liu et al., 1988). In the simplest case, as discovered by Coakley and Bretherton (1982), the 11 µm radiance's local standard deviation is plotted as a function of the local mean 11 µm radiance. The typical arch-like structure found in such plots comprises two distinct clusters of low standard deviation points, with a dispersion of high standard deviation points lying in between. The warmer cluster depicts the clear sky pixels while the colder cluster depicts the completely cloudy pixels. The dispersed points making up the arch are pixels that are partially cloud filled and exist as such because these pixels do not have the same degree of local coherence as those from completely clear or completely cloudy regions. Here, the cloud fraction increases as the local mean 11µm radiance decreases. The assumptions made when applying the spatial coherence method are that the clouds are optically thick and that they reside in distinct layers whose temperatures are appropriate to their altitude. Thus clouds such as thin cirrus (emissivity < 1) are poorly detected when spatial coherence is used alone. Moreover, clouds and surfaces which exhibit considerable spatial structure in the infrared (i.e. cirrus clouds, mixed land-water surface) tend to disrupt the identification of completely clear/cloudy regions due to the increased variance in the measurements (Sakellariou and Leighton, 1988).

The third class involves the use of sounder data. Multispectral infrared sounders are primarily used to estimate atmospheric temperature and composition profiles. However, they have been found to be very sensitive in detecting certain types of clouds, namely high clouds. Techniques making use of the potential that sounder data offers all start at the same set of radiative transfer equations. Given the atmospheric temperature and humidity profile, and the ground temperature, a set of N equation with N+2 unknowns are obtained. These unknowns are cloud fraction, cloud-top pressure, and N emissivities. To solve this set of equations, we can assume the emissivity to equal unity and solve for the apparent cloud fraction (the product of emissivity and cloud fraction). A more common approach is to assume the emissivity to be constant from one spectral band to the next. This requires closely spaced spectral channels, such as those found on sounder instruments where many channels are centered within the 15 µm CO<sub>2</sub> band. The methodology used in solving the set of equations is what distinguishes the sounder techniques amongst each other (i.e. Chahine, 1975; Smith and Woolf, 1976; Susskind et al., 1987; Eyre and Menzel, 1989). Wielicki and Coakley (1981) found that cloud retrieval errors using sounder techniques are minimum for high cloud types, making this an excellent cirrus cloud detection technique.

The fourth class uses IR discrimination, that is clear/cloudy discrimination is based on the differing wavelength dependences. Typically this method involves the construction of a two-dimensional histogram where the difference in brightness temperature between neighbouring channels are plotted against the brightness temperature of one of the channels (e.g. Inoue, 1987; Wu, 1987; Smith et al. 1988). The histogram is partitioned into regions identifying various cloud types and clear sky. This is usually done by constructing the frequency histogram of a test case and identifying those regions of high pixel density with the scene involved. The techniques differ in the IR channels used, data available, and inclusion of other visible channels (e.g. Inoue, 1987; Wu, 1987; Allen et al., 1990).

## 2.2 Validation of Satellite Cloud Detection Algorithms

A long-standing problem with satellite cloud detection algorithms is obtaining a proper method of validation (Rossow et al., 1985; Rossow 1989). This is due to the lack of a "truth" data set in which to compare the derived cloud cover. However, attempts are still made at validating the cloud detection algorithms. Table 2.2 lists the most recent attempts at validation with respect to cirrus cloud detection. Validation is made by intercomparing derived cloud cover with: (1) other satellite cloud detection algorithms; (2) cloud climatologies; (3) visual analysis of GOES VIS/IR satellite imagery; (4) surface observations of cloud amount; or some combination of the four. Let's look at these four separately.

### 2.2.1 Satellite Cloud Detection Algorithm Intercomparison

Intercomparison with other satellite cloud detection algorithms is not validation, rather, it is more of a consistency check that is somewhat valid if the comparison is made to an algorithm deemed rigid enough to be true (Diekmann and Smith, 1989). Intercomparison of a variety of algorithms has been carried out by Parker and Wielicki (1989). Lands at Thematic Mapper data was used to test the dependance of sensor spatial resolution on cloud amount. Their result for derived cloud amounts was that the amounts were only weakly dependent on the spatial resolution, with an increase of about 6% on average, from 1 km to 8 km, for all cloud algorithms. The most striking result, however, was the difference in derived cirrus cloud amounts, especially between the ISCCP (Rossow et al., 1985) and the NCLE (Stowe et al., 1988) algorithms. The NCLE

Table 2.2. Summary of intercomparison of algorithms recently made with reference to cirrus.

Algorithms	References
Dynamic IR threshold (Coakley, 1987), Fixed IR threshold, and Spatial Coherence Method (Coakley and Bretherton, 1982)	
Cluster Technique (Desbois and Seze, 1984) with surface observations	· ·
Cluster Technique (Seze and Desbois, 1987) with VIS, IR, and VIS+IR threshold (Seze and Desbois, 1987)	
IR sounder (Susskind <i>et al.</i> , 1987), IR threshold (Stowe <i>et al.</i> , 1984), and GOES qualitative	Susskind et al., 1987
NCLE (Stowe <i>et al.</i> , 1988), ISCCP (Rossow, <i>et al.</i> , 1985), and various climatologies.	
HBTM (Minnis et al., 1987) applied to GOES and the Reflectance Threshold Technique (Wielicki and Welch, 1986) applied to Landsat	Minnis and Wielicki, 1988
NCLE (Stowe <i>et al.</i> , 1988) and GOES qualitative	Stowe et al., 1988
ERBE MLE (Smith <i>et al.</i> , 1986) and bispectral radiative transfer models to AVHRR (Diekmann and Smith, 1989)	Diekmann and Smith, 1989
Hybrid Histogram-Spatial Coherence Method (Ebert, 1989) with surface observations	
NCLE (Stowe <i>et al.</i> , 1988), ISCCP (Rossow <i>et al.</i> , 1985), and various climatologies	
IR threshold, VIS threshold, ISCCP (Rossow et al., 1985), HBTM (Minnis et al., 1987), NCLE (Stowe et al., 1988), Spatial Coherence Method (Coakley and Bretherton, 1982), and Functional Box	
Counting (Lovejoy et al., 1987)	
ISCCP with surface observations	Whitlock et al., 1989
ISCCP, NCLE, and cloud climatology	Rossow and Schiffer, 1991

underestimated the ISCCP cirrus cloud amount by about 40%. Others reported similar, but not as drastic comparison between NCLE and ISCCP. Hwang et al. (1988) reported a 14% difference in total cloud amount averaged globally; Stowe et al. (1989) reported a 15% difference, and Rossow and Schiffer (1991) reported a 10% difference. Note, however, that the latter reports are for total cloud amount rather than cirrus cloud amount. A difference was expected since the IR threshold window for the NCLE is twice as large as ISCCP (6 K compared to 3 K). Stowe et al. (1989) reported that doubling the ISCCP threshold window brings the total cloud amount predicted by the two algorithms within 1% when globally averaged (with differences as high as 15%). Results from Seze and Desbois (1987) also found that a 6 K threshold window best matched the cloud retrieval of their improved cluster technique. Parker and Wielicki (1989) reported that for cirrus cloud detection, the simple IR threshold agrees very well with the ISCCP algorithm. This indicates the dominance of the IR threshold section of the ISCCP algorithm in the presence of cirrus clouds. Classically, however, the IR thresholding technique performs poorly when applied to thin cirrus classification. These thin cirrus typically have emissivities less than one (Platt et al., 1980) and as a result are often misclassified as middle or low clouds based on IR detection alone (Goodman and Henderson-Sellers, 1988).

The IR sounder technique of Susskind et al. (1987) underestimates total cloud amount on average by 10% (but as high as 30%) compared to the retrieval by IR thresholding. Several reasons may exist. Firstly, the IR sounder technique measures the apparent cloud fraction (the product of emissivity and cloud fraction) rather than cloud fraction. The measured

apparent cloud fraction will generally have lower values compared to the cloud fraction. Secondly, the IR threshold assumes fully clear or fully cloudy pixels. Misclassification of sub-pixel cloudiness as overcast often occurs when using IR thresholding, thus overestimating the true cloudiness. Thirdly, IR sounder techniques perform poorly in detecting low clouds (Wielicki and Coakley, 1981; Eyre and Menzel, 1989). This is also true, however, for IR thresholding (Parker and Wielicki, 1989). The difference in magnitude between each algorithm is not known. Unfortunately Susskind et al. (1987) did not compare the high cloud amount with the IR thresholding high cloud amount. However, given the above information, it is expected that the IR thresholding would have underestimated the cirrus cloud amount as compared to the IR sounder technique. This would also be consistent with the expected underestimation of cirrus cloud amount using IR thresholding due to misclassification because of variable cirrus emissivity.

The dynamic IR threshold technique (Coakley, 1987) and the spatial coherence method (Coakley and Bretherton, 1982) underestimate the fixed IR threshold technique by 20% when applied to middle and high clouds (Coakley, 1987). Coakley's goal was to alleviate the problem of subpixel clouds being misclassified as either clear or overcast when using the fixed IR threshold. The dynamic IR threshold works as well as the spatial coherence method (SCM) and requires the same assumptions (as described in section 2.1), except that the dynamic IR threshold technique does not require pixels to be completely covered or cloud-free somewhere in the scene. However, the SCM works poorly for cirrus clouds due to the considerable spatial structure these clouds exhibit. This is also shown

in the results of Parker and Wielicki (1989) where cirrus clouds are underestimated by about 35% using the SCM compared to the fixed IR threshold. This large difference is also due in part to some mixed scenes (land/water) used in Parker and Wielicki's investigation. Sakellariou and Leighton (1988) found that under mixed scenes the SCM works extremely poorly. Thus apart from alleviating the sub-pixel cloud misclassification of fixed IR thresholding techniques, the SCM and the dynamic IR threshold method would still underestimate cirrus cloud amounts due to the assumptions made in applying the algorithms.

Another technique which makes use of the spatial coherence method is the Hybrid Histogram-Spatial Coherence Method (HHSCM) of Ebert (1989). The HHSCM was compared to three different thresholding techniques over polar regions: (1) a simple bispectral (VIS/IR) threshold, (2) the same bispectral threshold with classification, and (3) classification with a class-optimal threshold channel determined by her study. Classification using a pattern recognition technique (Ebert, 1987) was performed before the application of the HHSCM and threshold techniques. She found that the HHSCM performed better than the thresholding techniques for cirrus, cirrocumulus, and altocumulus, but not for cirrostratus and altostratus, over all surface types. In cases where the classification was in error, large errors in derived cloud cover were encountered, especially in cases involving thin stratus and thin cirrus. Her most impressive result, however, was the improvement of cloud detection using thresholding when the scene was first classified; on average the results improved by 25%.

The Hybrid Bispectral Threshold Method (HBTM of Minnis et al., 1987) underestimates the IR threshold-derived cirrus amounts by about 15% (Parker and Wielicki, 1989). This is consistent with the findings of Minnis and Wielicki (1988) that the HBTM slightly underestimates cirrus cloud amounts. However, this was estimated by comparing the HBTM, applied to GOES VIS/IR data, to the Reflectance Threshold Technique (Wielicki and Welch, 1986) using Landsat data. As noted by Minnis and Wielicki (1988), the absolute accuracy of the Landsat-derived cloud cover is unknown for cirrus clouds due to the cloud's low reflectance. Given the nature of reflectance techniques to underestimate cirrus clouds (Parker and Wielicki, 1989), the HBTM is believed to do no better.

Finally, according to the results of Parker and Wielicki (1989), Functional Box Counting (Lovejoy et al., 1987) underestimates cirrus cloud amounts by about 30% compared to IR threshold. This is because the scale invariant power law does not apply to cirrus clouds at all spatial scales. In Parker and Wielicki's results, breaks were found in the scale invariant power law between 2 - 4 km for cirrus clouds. If this is so, the scale invariant assumption does not apply to cirrus clouds, and thus, Functional Box Counting should not be used for their detection.

## 2.2.2 Validation using GOES Imagery

One other method of validating a cloud detection algorithm is to compare the retrieved cloud amounts to the cloud amounts derived from an analyst interpretation of GOES VIS/IR imagery. In the visible imagery thick clouds are bright, while thin clouds such as cirrus are fainter. The

infrared imagery assigns a brightness value according to the difference between the observed temperature and the warmest temperature in the scene; thus, high clouds appear bright while low clouds and clear cool surfaces appear faint. Snow covered regions are the most difficult areas to verify because snow and clouds are both bright in the visible and cold in the infrared. An analysis of the uncertainties involved in using an analyst to derive cloud amount has been assessed by Stowe (1984). He found that the random error involved in estimating high cloud amount and total cloud amount are as high as 18% and 14%, respectively, over snow-free regions.

Both Stowe et al. (1988) and Susskind et al. (1987) have used this approach for validation (ref. Table 2.2). Stowe et al. (1988) has reported that the total cloud amount derived using the NCLE algorithm is in general agreement with the GOES analyst. However, errors as large as 50% have been noted in a few regions. High cloud amount comparisons were not noted. Susskind et al. (1987) has shown that high cloud amounts derived from the IR sounder technique compare well with the derived high cloud amounts from the GOES analyst. Moreover, the IR sounder technique also retrieves clouds over snow-covered areas.

## 2.2.3 Validation using Cloud Climatologies

Another popular method for validating a cloud detection algorithm is to compare derived cloud amounts to existing cloud climatologies<sup>b</sup>. Validation of the NCLE algorithm using this approach was carried out by Hwang et al. (1988) and Stowe et al. (1989). Hwang et al. (1988) com-

pared the NCLE-derived total cloud amount for July 1979 to climatological July total cloud covers taken from (1) London (1957), (2) Beryland and Strokina (1980a,b), and (3) the US Air Force 3DN for July 1979 as analyzed by Hughes and Henderson-Sellers (1985). London (1957) used 10 years of surface cloud observations in the northern hemisphere to derive his climatology. Beryland and Strokina (1980a,b) used 30 years of surface observations, with some satellite cloud observations included in the later years. The US Air Force 3DN, as analyzed by Hughes and Henderson-Sellers (1985), used a combination of surface, aircraft, and satellite cloud observations. Apart from polar regions, the NCLE-derived total cloud cover shows the same zonally averaged trends, for July 1979, as the other climatologies. However the magnitudes differ, with the NCLE zonally averaged total cloud amount extrema being larger than the climatologies. Globally, the NCLE total cloud cover underestimates the 3DN total cloud cover analysis by 6%, with a maximum zonal underestimate of 17%. No high cloud comparisons were made. Stowe et al. (1989), however, did make the high cloud comparison for the same month and year. They reported that comparison with the 3DN-derived high cloud amounts, as analyzed by Henderson-Sellers (1986), agrees well with the NCLE high cloud amounts in both regional distributions and approximate magnitudes. I made the comparison and noted that this was true. But careful extrapolation between the even-labeled contours of Henderson-Sellers (1986) and the odd-labeled contours of Stowe et al. (1989), for

bThe 30 year standardized period for a defined climatology (WMO, 1971) has not been employed in this chapter. Instead various time intervals will be specified for the climatology.

the northern hemisphere tropics and mid-latitudes, reveals that the NCLE-derived high cloud amount underestimates the 3DN-derived high cloud amount by about 5 to 10%. Stowe et al. (1989) also compared the NCLE high cloud amounts to the high cloud climatology of Barton (1983). Barton (1983) reported a climatology for clouds higher than 6 km, based on two narrow-band measurements in the 2.7 µm absorption band of carbon dioxide and water vapor, using the Selective Chopper Radiometer (SCR) on Nimbus-5. The climatology was for June-July-August averaged over 1973 and 1974. The comparison showed that Barton's high cloud amounts were generally 10% higher than the NCLE high cloud amounts, with the regional distributions being in good agreement. Stowe et al. (1989) attributed the difference in magnitude to be in part due to the misclassification of thin cirrus clouds by the NCLE as mid- or low-level, and in part due to the high cloud altitude definition being 1 km higher for the NCLE algorithm.

Woodbury and McCormick (1986 have also made observations of high clouds using the Stratospheric Aerosol and Gas Experiment (SAGE) data for the period of February 1979 to November 1981. The SAGE utilizes a solar occultation technique to measure aerosol extinction profiles. Anomalously high extinction values are attributed to cirrus clouds since the SAGE has a maximum observational penetration down to about 7 km above the Earth's surface. The sensitivity to extinction values of the SAGE allows it to make measurements of very thin cirrus clouds which normally go undetected by surface observers and sounding techniques (Liou, 1986). Consequently, appropriate validation of the SAGE cirrus retrieval still needs to be carried out. The results of Woodbury and

McCormick (1986) found that the SAGE cirrus frequency of occurrence amounts are up to twice as high as Barton's SCR amounts. This being the case, it would be reasonable to assume that the NCLE algorithm underestimates high cloud amounts because of its inability to detect thin cirrus clouds.

Rossow and Schiffer (1991) compared the ISCCP-derived total cloud amount with the cloud climatology of Warren et al. (1988). This climatology was derived from surface observations over a ten year period from 1971 to 1981. The comparison showed that the ISCCP algorithm underestimated climatology by about 5% in total cloud amount. Since they also showed that the NCLE underestimated the ISCCP-derived total cloud amount, it follows that the NCLE also underestimates the total cloud amount climatology of Warren et al. (1988).

#### 2.2.4 Validation using Surface Observations

"The most readily available method of validation (and perhaps the only conceivable one) lies in comparison with surface synoptic reports..." (Goodman and Henderson-Sellers, 1988). We must realize, however, that cloud cover estimation is made from two different points of view: from space looking down and from the surface looking up. Because of differing amounts of cloud sides viewed from each point, it is expected that different estimates of cloud amounts be derived in cases of broken cloudiness involving a significant amount of vertical development. Empirical relationships have been derived to take this effect into account (e.g. Malick et al., 1979). In multi-layered situations, satellites tend to

underestimate low-cloud amounts and surface observers tend to underestimate high-cloud amounts (Henderson-Sellers et al., 1987). This is due to the obscuration of view provided by the cloud layer closest to the view points. In terms of cirrus cloud cover, surface observers have the advantage of detecting thin cirrus clouds where many satellite retrieval techniques may fail to detect them (Henderson-Sellers, 1987). Moreover, surface observers are not confused by mixed surface scenes, whereas these types of scenes are confused by many satellite cloud algorithms.

Surface observers do have limitations. The uncertainty in deriving high cloud amount is approximately 10% based on the comparison between visual observations and all sky photographs (Merritt, 1966). However this does not take into account the very thin cirrus clouds that may be missed by both types of surface observations. Perhaps the largest limiting factor in using surface observations to validate satellite cloud algorithms is their poor spatial coverage of the Earth, especially over the oceans. Many cloud algorithms rely on spatial uniformity of the surface for successful cloud retrieval. Because of this, oceanic regions offer an excellent test site in which to validate the cloud algorithms. Moreover, with oceans covering about 70% of the globe, it is imperative that we know the accuracy of these cloud algorithms over ocean. Sadly, the few ship reports of cloud cover, coincident with satellite measurements, do not offer a large enough data base to appropriately validate the cloud algorithms.

Few satellite cloud algorithms are verified using surface observers.

Table 2.2 lists those who have made the attempt. Henderson-Sellers et al.

(1987) compared the clustering technique of Desbois and Seze (1984)

with surface observations. They found that high cloud amounts are in agreement 35% of the time. However 95% of this value is for completely clear or completely cloudy scenes. Another 50% of the observations are within ± 1 okta (about 12% of cloud coverage). An attempt by Whitlock et al. (1989) to compare cloud coverage between the ISCCP algorithm and surface observations lacked any quantitative conclusions due to the satellite pixel to ground station navigation mismatch. A qualitative conclusion was that the ISCCP algorithm tended to have difficulties detecting thin clouds. The HHSCM (Ebert, 1989) was also compared to ground observers, but only for one day in which there was only 5% cirrus cloud cover. The HHSCM was reported to detect these cirrus clouds. However manual nephanalysis has shown that high clouds analyzed using the HHSCM carried a mean absolute error averaging about 23%.

#### 2.3 Discussion

One of the major problems remaining in determining the accuracy of derived cloud fraction is defining what exactly constitutes a cloud. The term accuracy is defined as "in exact conformity to truth or to some standard" (Gove, 1986). Because a proper definition (i.e. standard) of what constitutes a cloud does not presently exist, the accuracy of a cloud detection algorithm becomes somewhat vague. A criterion which defines a cloud is needed. Perhaps by looking at, say, the effects on both longwave and shortwave radiation, the effects of sensor resolution, and the cloud microphysics (i.e. drop size distribution, total liquid water amount, phase, etc.), it may be possible to assign a threshold on defining cloud vs no-cloud. Such a threshold would be useful in that it would give the cloud detection validation a basis with which to work. Since this is not done in practice, intercomparison of derived cloud amounts between methods is inherently subject to undefined uncertainties. This is especially true for cirrus clouds, since thin clouds of this category may often skim the line of detection within most of the cloud detection methods. For example the cirrus cloud occurrences derived from SAGE data (Woodbury and McCormick, 1986) register thin cirrus clouds that would be considered "invisible" to the naked eye and other cloud detection methods. Do the thin cirrus clouds derived from SAGE data meet the criterion of "cloud"? Until we can answer this question, it would be erroneous to compare the magnitude of SAGE-derived cirrus cloud amounts to that of other retrieval techniques.

The focus of this chapter was on the performance of recent cloud detection algorithms in detecting cirrus clouds. This was done by compar-

ing retrieved cloud amounts to other cloud detection algorithms, cloud climatologies, visual analysis of GOES VIS/IR satellite imagery, and surface observations. Apart from the lack of a cloud definition, some of these methods still have inherent problems associated with their method of validation.

Comparing satellite retrieved cloud amount to cloud amount derived from surface observations is considered an appropriate method of validation by "truth" (Goodman and Henderson-Sellers, 1988). But uncertainties still exist in surface observations. As discussed previously, surface observations and satellite observations of cloud amount will differ because of the differing points of view (i.e. looking up from ground vs looking down from space). Moreover the sensitivity of the eye in detecting thin cirrus clouds still plays a role in determining cloud amount. There is one other important difference amongst surface observations: the observer's psychological interpretation of the sky shape. It has been well documented that surface observers overestimate the angular distance between two points in the sky when they are fairly close to the horizon as compared to the same two points when they are closer to the zenith (McGuffie and Henderson-Sellers, 1989). McGuffie and Henderson-Sellers (1989) concluded that cloud amounts (as well as cloud types) derived from the analysis of all sky photographs depend on the shape of the camera lens used in projecting the sky onto film. This is due to the differing perception of the shape of the sky-dome. Because the human perception of the shape of the sky-dome remains unknown, differences in derived cloud amounts from surface observers and surface all-sky photographs are expected. Uncertainties of these methods are typically quoted at about 10% (Merritt, 1966; Holle and Mackay, 1975).

The most questionable method of validation is to compare derived cloud amounts with past cloud climatologies. Because of the seasonal and interannual variability of the climate system, it is hardly appropriate to compare the magnitude of the average monthly cloud amount from one year to that of past years; though similar geographic and seasonal cloud amount variations are reasonable. The methods used to derive cloud climatologies also introduce uncertainties in the intercomparison; for example, high cloud climatologies of Woodbury and McCormick (1986) and Barton (1983) differ in magnitude up to 50%. This is because of the differing sensitivity in retrieving thin cirrus clouds. Problem regions can also have a large effect on the intercomparisons. For example, Stowe et al. (1989) found that the NCLE-derived climatology was different in polar regions as compared to other climatologies. This was because of the problems the NCLE algorithm has in detecting clouds over polar regions due to the similar spectral signatures the clouds and snow exhibit in the visible and infrared (Stowe et al., 1989).

The sample size is another problem inherent to all methods of intercomparison. If one is to quote retrieved cloud amount differences between methods, it is imperative that the retrieved cloud amounts be over a
broad enough area or over a sufficient period of time to encompass all
scene type scenarios. The literature reveals a large amount of one day
comparisons (e.g. Ebert, 1989). This is not sufficient for validation as it
does not encompass, say, the large variability in optical properties that
cirrus clouds possess. Indeed the literature reveals that the greater the

difference in space and time sampling used, the greater the difference in derived cloud cover that may exist between the validation of the two methods (e.g. ISCCP vs NCLE between Stowe et al. (1989) and Parker and Wielicki (1989)).

With the above discussion in mind, this review has revealed that techniques which derive cloud top pressure using sounder data are best suited for detecting cirrus clouds compared to the other techniques listed in Table 2.1, based on sensitivity of detection and classification of thin cirrus clouds. Moreover, these techniques are capable of deriving cirrus cloud amounts over snow/ice covered regions. Keep in mind that the derived cloud amount is actually the effective cloud fraction (the product of emissivity and cloud fraction); but without a proper cloud definition, the effective cloud fraction is just as valid. The major disadvantage of these techniques is the poor spatial resolution (> 18 km) of IR sounders.

Those which have undergone the largest validation efforts have been the techniques using some form of IR thresholding. In particular the validation of the simple IR threshold, the NCLE, and the ISCCP algorithms have been the focus of many scientists' efforts. The conclusion is that these techniques are highly sensitive to the IR threshold window chosen. This has been noted for some time now (e.g. Rossow et al., 1985). Even though the NCLE and ISCCP algorithms use a visible channel for additional information, the IR thresholding section of these algorithms dominate over the visible thresholding section when cirrus clouds are involved. This is due to the large contrast between cirrus cloud and surface in the infrared as compared to the visible channel. When the same IR threshold window is used for the IR, NCLE, and ISCCP algorithms, all

retrieve approximately the same amount of cirrus clouds (Stowe et al., 1989). These techniques all underestimate cirrus cloud amounts compared to the sounder techniques. A major reason is that algorithms such as ISCCP classify clouds based on the retrieved brightness temperature. Thus clouds, such as cirrus, with emissivities less than one are often classified lower than their actual height. Sounder techniques retrieve cloud top pressure and leave the emissivity problem to the definition of cloud fraction.

The other cloud detection algorithms, listed in Table 2.1, did not perform as well as ISCCP in deriving cirrus cloud amounts, based on validation of retrieved cloud amounts. The HHSCM algorithm (Ebert, 1989) requires further validation of cirrus cloud retrievals, but thus far it seems to perform as well as the ISCCP algorithm. Those which use IR discrimination (as defined in Table 2.1) are not well validated. Therefore a measure of their performance is not given here.

To summarize, this chapter highlights two basic steps that must be taken in order to obtain accurate cirrus cloud climatologies. The first is a call for a cloud definition. If any measure of accuracy is to be identified amongst cloud detection algorithms, this step must be taken. The second calls for a proper understanding of the validation strategies available and that correct validation be made over sufficient space or time scales. In light of the above discussion, it appears that ISCCP's goal of  $\pm 5\%$  on cirrus cloud amounts (30 day averages) (Schiffer and Rossow, 1983) cannot be currently ascertained.

#### CHAPTER 3

# A New Cloud Detection Technique using the

#### Multi-angle Imaging SpectroRadiometer

### 3.1 The Multi-angle Imaging SpectroRadiometer

The Earth Observing System (EOS) (NASA, 1991) is a program which will carry out multidisciplinary Earth science studies with the aid of a variety of remote sensing instruments (Dozier, 1991). The Multi-angle Imaging SpectroRadiometer (MISR) (JPL, 1990; Diner, 1989) is one such instrument and will provide multi-angle continuous coverage of the Earth at nine discrete view angles. This is achieved by allocating a separate camera for each viewing direction. One camera points at nadir, four point in the forward along-track direction, and four point in the backward along-track direction. The optics of each camera are adjusted to give the same cross-track resolution of 240 m in the Local Mode and 1.92 km in the Global Mode. The 360 km swath width and its 705 km sun-synchronous orbit allows complete global coverage every 9 days and a polar coverage every 2 days. Images from each camera will be obtained in a pushbroom fashion in four spectral bands ranging from 0.44 μm to 0.86 μm.

MISR, which is scheduled for launch in 1998 on the NASA a.m. cluster, is the only instrument for EOS that will provide multi-angle continuous coverage of the Earth, with multi-angle observations of each tar-

get area within a time scale of several minutes. Therefore, multi-angle measurements of the same target area are made under the same atmospheric conditions. In the context of this study, this unique feature is used to derive a new cirrus cloud detection algorithm. The MISR instrument specifications, important for the derivation of the cirrus cloud detection algorithm, are summarized in Table 3.1.

Table 3.1. MISR Instrument Specifications

Instrument Parameters	Specification	Notes
Camera Geometry	·	
Number of Cameras	9	1 nadir, 4 fore, 4 aft
Surface View Angles	0°, ± 26.1°, ± 45.6°, ± 60°, ± 70.5°	The surface view angle is defined as the angle between the Earth's surface local normal vector and the vector at the surface pointing in the direction of the camera.
Camera Offset Angle	Included	For an ascending(descending) orbit the fore cameras are offset to the west(east), and the aft cameras are offset to the east(west). This corrects for swath misalignment do to the Earth's rotation.
Orbit		
Туре	Sun-Synchronous	
Inclination	98.186°	
Period	98.88 min.	
Altitude	705 km	Actual range is from 704 km to 732 km.
Image Characteristics		
Swath Width	356 km	20 km swath overlap included.
Cross-Track Dimension	240 ± 5 m	
Down-Track Dimension	240 m average	
Line Repeat Time	35.6 msec	
Pixel Averaging	Yes	Local Mode has no pixel averaging (240 m resolution). Global Mode has 8x8 pixel averaging (1.92 km resolution).
Spectral Bands		
Central Wavelengths (nm)	443, 550, 670, 860 <sup>c</sup>	± 2 nm
Maximum Allowable Bandwidth (nm)	40, 20, 20, 60	
Radiometric Calibration		For a uniform, 100% reflectance
Requirements <sup>d</sup>		Lambertian target.
Absolute Radiometric Accuracy	± 3 %	
Camera-to-Camera Relative Accuracy at a given wavelength	± 1 %	
Band-to-Band Relative Accuracy for a single camera	± 0.5 %	
Pixel-to-Pixel Relative Accuracy for a single detector array	± 0.7 %	

<sup>&</sup>lt;sup>c</sup>The 860 nm centered wavelength has since been moved to 865 nm.

<sup>d</sup>The calibration uncertainty has since been derived. It has not affected the general conclusions of this chapter, but it does affect the details slightly.

# Ì

# 3.2 A New Cloud Detection Algorithm

Many satellite cloud detection algorithms exist which can be applied globally to determine cloud amounts. As we have seen in Chapter 2, many of these algorithms work poorly in detecting cirrus clouds, especially thin cirrus, owing to the clouds variable emissivity and low reflectance. This chapter deals with the development of a new cirrus cloud detection algorithm which makes use of the multi-angle viewing capability of MISR. The new algorithm combines two separate techniques. The first applies a Predetermined Clear Sky Threshold (PCST) which quickly identifies clear sky regions from regions that may be contaminated by clouds. The second technique takes these contaminated regions and determines their Band-Differenced Angular Signature (BDAS). The BDAS discriminates between upper level clouds (cirrus) and lower level reflectance anomalies (such as surface fogs, ocean white caps, etc.). These techniques are developed using an atmospheric radiative transfer model to provide simulated topof-the-atmosphere (TOA) radiances. Since about 70% of the Earth's surface is ocean, the atmospheric model is coupled to an ocean surface model. Future work will extend this study to include land surfaces.

# 3.2.1 The Atmospheric Model

The atmospheric model used in providing simulated results is LOWTRAN 7 (Kneizys et al., 1988). LOWTRAN 7 is a low resolution propagation model and computer code for predicting atmospheric transmittance and background radiance at a resolution of 20 cm<sup>-1</sup> with a range of 0 to 50000 cm<sup>-1</sup>. The code uses a single-parameter band model for

molecular line absorption, and includes the effects of continuum absorption, molecular scattering, and aerosol extinction. The following are highlights of this model:

- A spherical refractive atmosphere (Gallery et al., 1983; Kneizys et al., 1983) to take into account the spherical geometry of the earth-atmosphere system.
- A multiple scattering parameterization (Isaacs et al., 1987) based on the two stream approximation and an adding method for combining atmospheric layers.
- A choice of six reference atmospheres, each defining temperature, pressure, density, and mixing ratios for H<sub>2</sub>O, O<sub>3</sub>, CH<sub>4</sub>, CO, and N<sub>2</sub>O, all as a function of altitude, which allows the user a range of climatological choices (selected from NASA, 1966, and NASA, 1976).
- A choice of ten boundary layer aerosol models to choose from (Kneizys et al., 1988; Kneizys et al. 1980) which allows for user-defined meteorological visibility ranges.
- A choice of eight cloud types (Kneizys et al., 1988; Kneizys et al., 1983; Shettle et al., 1988), three of which are ice clouds, which allows the user to choose cloud altitude, cloud thickness and cloud optical thickness.

The LOWTRAN 7 surface is Lambertian with a user defined albedo. In order to obtain more realistic results, the Lambertian surface was replaced by a flat ocean model surface (Section 3.2.2). The method of replacement will be described in Section 3.2.3.

#### 3.2.2. The Ocean Model

This section describes the flat ocean model used to replace the LOWTRAN 7 Lambertian surface. In section 3.2.4, the choice of a flat ocean model as opposed to a rough-surface ocean model will be discussed.

Consider Figure 3.1. The reflectivity between the two transparent media having a flat boundary is given by the Fresnel reflectivity coefficient:

$$\rho_{12} = \frac{1}{2} \left[ \frac{\sin^2(\theta_1 - \theta_2)}{\sin^2(\theta_1 + \theta_2)} + \frac{\tan^2(\theta_1 - \theta_2)}{\tan^2(\theta_1 + \theta_2)} \right]$$
(3.1)

where  $\theta_1$  and  $\theta_2$  are the angles of the incident and refracted ray, measured from the boundary's normal, of medium 1 (with refractive index  $m_1$ ) and medium 2 (with refractive index  $m_2$ ), respectively.  $\theta_1$  and  $\theta_2$  are related via Snell's law:

$$m_1 \sin \theta_1 = m_2 \sin \theta_2 \tag{3.2}$$

Since we are interested in radiance measurements, the change in radiance as the radiation crosses from medium 1 to medium 2 must be computed. The radiance, L, is the irradiance, dE (Wm<sup>-2</sup>), per unit solid angle,  $d\Omega$ , at some angle  $\theta = \cos^{-1}\mu$  from the surface normal. Thus,

$$L_1 = \frac{dE_1}{\mu_1 d\mu_1 d\phi_1}, \qquad L_2 = \frac{dE_2}{\mu_2 d\mu_2 d\phi_2}$$
 (3.3)

where  $\phi$  is the azimuth angle. From continuity arguments, the irradiance from medium 1 to medium 2 is related by

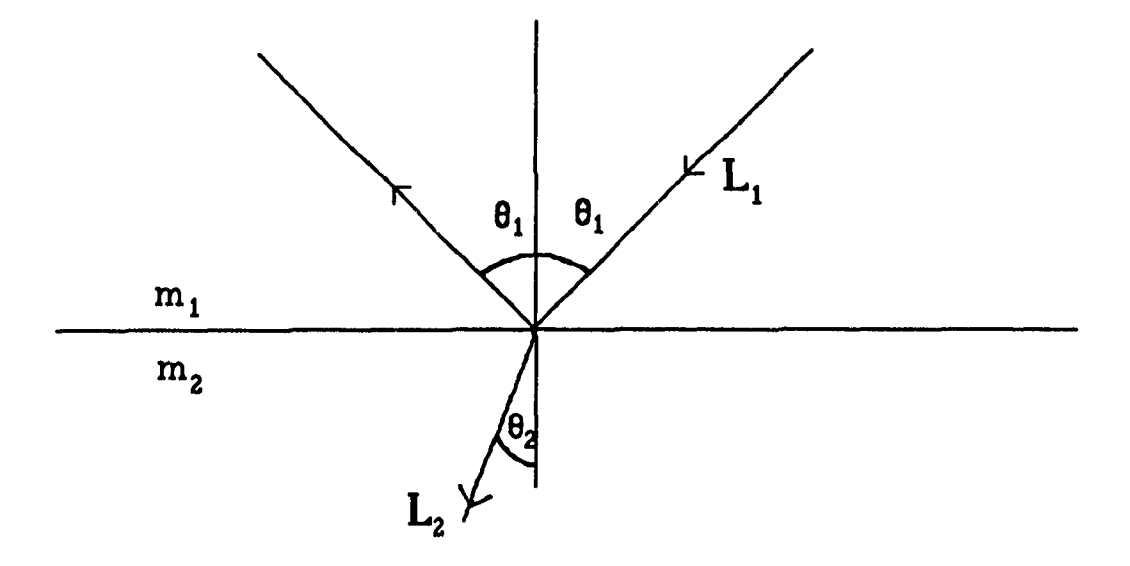


Figure 3.1. Flat surface depiction for Fresnel's equation applications.

$$dE_2 = (1 - \rho_{12})dE_1$$

Substituting this expression into (3.3) yields, with  $d\phi_1 = d\phi_2$ ,

$$(1 - \rho_{12})L_1\mu_1 d\mu_1 = L_2\mu_2 d\mu_2 \tag{3.4}$$

From Snell's law (equation 3.2), it's easy to show that

$$\mu_2 d\mu_2 = \left[\frac{m_1}{m_2}\right]^2 \mu_1 d\mu_1 \tag{3.5}$$

Substituting equation (3.5) into (3.4) and rearranging yields

$$L_2 = \left[\frac{m_2}{m_1}\right]^2 (1 - \rho_{12}) L_1 \tag{3.6}$$

Equation (3.6) is sometimes referred to as the interfacial radiance equation.

The flat ocean model is depicted in Figure 3.2. The incoming radiation, L<sub>i</sub> (which is obtained from LOWTRAN 7), interacts with the flat ocean surface according to equations (3.1), (3.2), and (3.6). The refractive index of air and water are taken to be  $m_a = 1.00$  and  $m_W = 1.33$ , respectively, throughout the MISR spectral range. The reflected radiance, L<sub>f</sub>, is simply given by

$$L_f(\mu_i) = \rho_{aw} L_i(\mu_i) \tag{3.7}$$

and the refracted radiance, Ld, is given by

$$L_{d}(\mu_{r}) = \left[\frac{m_{w}}{m_{a}}\right]^{2} (1 - \rho_{aw}) L_{i}(\mu_{i})$$
(3.8)

Some of this refracted radiation is backscattered, the amount strongly depending on the wavelength of radiation due to the concentrations of phy-

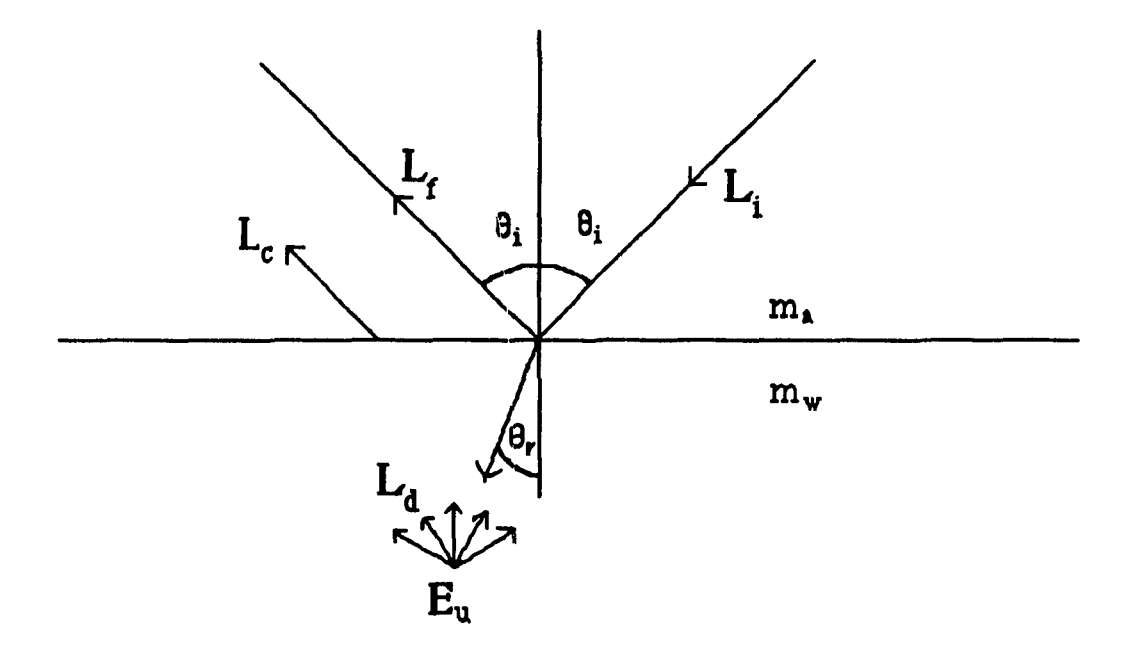


Figure 3.2. Ocean model depiction for upwelling radiation calculations.

toplankton, yellow substance, and sediments. Measurements of such reflectance, R, defined as

$$R = \frac{E_u}{E_d}$$

where  $E_u$  and  $E_d$  are the upwelling and downwelling irradiance, respectively, just below the sea surface, have been made (Sathyendranath and Morel, 1983) and are shown in Figure 3.3. If the backscattered radiance,  $L_u$ , is isotropic then

$$L_{u} = \frac{RE_{d}}{\pi} \tag{3.9}$$

Austin (1980) found that the isotropic assumption is not valid when the radiance measurement of  $L_u$  is made at nadir; a valid approximation is to replace  $\pi$  with a value, call it Q, of about 5 in equation (3.9). From equation (3.3) Ed is given by

$$E_{d} = \int_{0}^{2\pi} \int_{0}^{1} L_{d}(\mu_{r})\mu_{r}d\mu_{r}d\phi$$

Substituting Li for Ld (equation 3.8) yields

$$E_{d} = \int_{0}^{2\pi} \int_{0}^{1} \left[ \frac{m_{w}}{m_{a}} \right]^{2} (1 - \rho_{aw}) L_{i}(\mu_{i}) \mu_{r} d\mu_{r} d\phi$$

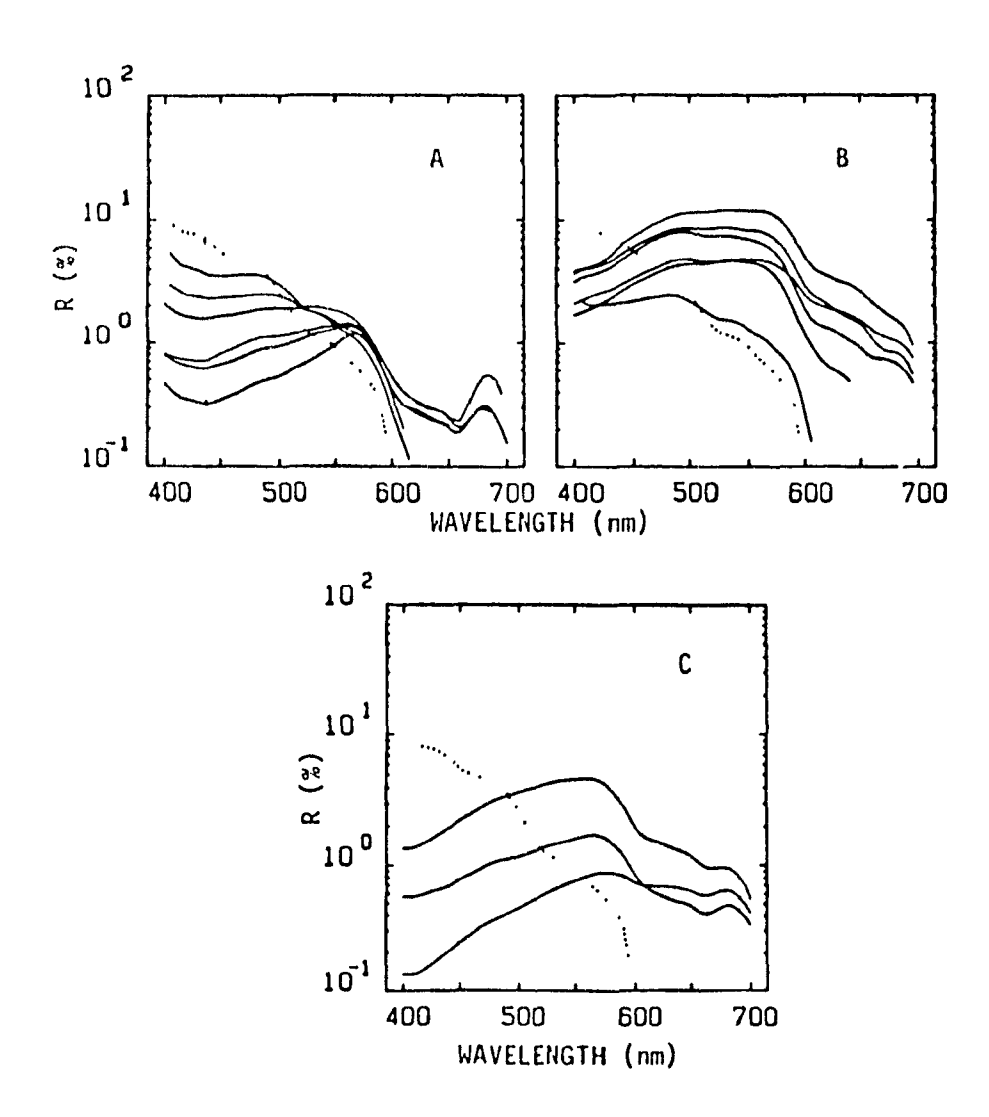


Figure 3.3. R values for different waters: (A) phytoplankton dominated, (B) suspended sediment dominated, (C) yellow substance dominated. The dotted line is for clear ocean water. (taken from Sathyendranath Morel, 1983)

and with the aid of equation 3.5 this becomes

N. C.

$$E_{d} = \int_{0}^{2\pi} \int_{0}^{1} (1 - \rho_{aw}) L_{i}(\mu_{i}) \mu_{i} d\mu_{i} d\phi$$
 (3.10)

The upwelling radiance,  $L_u$ , also interacts with the air-water interface. The interfacial radiance equation for  $L_u$  is written as

$$L_{c}(\mu_{i}) = \left[\frac{m_{a}}{m_{w}}\right]^{2} (1 - \rho_{wa}) L_{u}(\mu_{r})$$
(3.11)

L<sub>c</sub> is often called the ocean colour. Combining equations (3.10) and (3.8) into (3.11) yields

$$L_{c}(\mu_{i}) = \left[\frac{m_{a}}{m_{w}}\right]^{2} (1 - \rho_{wa}) \frac{R}{Q} \int_{0}^{2\pi} \int_{0}^{1} (1 - \rho_{aw}) L_{i}(\mu_{i}) \mu_{i} d\mu_{i} d\phi$$
(3.12)

Finally, the total contribution to the satellite-measured radiance, before atmospheric corrections are made, is simply the sum of L<sub>f</sub> (equation 3.7) and L<sub>c</sub> (equation 3.12).

# 3.2.3. Atmosphere-Ocean Model Coupling and Verification

The LOWTRAN 7 Lambertian surface does not describe the reflection pattern of an ocean surface with any great realism. Thus it was necessary to replace the Lambertian surface with a more realistic ocean model, such as the one described above. In doing so, some of the interactions between LOWTRAN 7's atmosphere and its Lambertian surface were not preserved. To understand this, it is first necessary to discuss several contributions to the satellite-measured radiance. These are depicted in Figure 3.4. The possible pathways are (not including the ocean colour contribution):

- $-L_0$  = the direct beam reflected by the ocean surface to the satellite without scattering.
- Lao = the diffuse radiation reflected by the ocean surface to the satellite without scattering.
- $L_{0a}$  = the direct beam reflected by the ocean surface and then scattered to the satellite.
- $L_a$  = the direct beam is scattered back to the satellite by the atmosphere without reflection by the surface.
- $L_m$  = the radiation has undergone multiple reflection with the surface.

The magnitude of each term depends strongly on the solar zenith angle (SZA). This is because the surface reflection coefficient and the atmospheric pathlength through which the direct beam traverses are functionally dependant on the SZA. The top of the atmosphere (TOA) radiances depend on both the solar and viewing geometries; i.e.  $L_{c,t} = L_{Sat}(\mu, \mu_O, \phi_r)$ , where  $\mu_O$  is the cosine of the SZA and  $\phi_r$  is the relative azimuth angle (RAZ) between view and sun. LOWTRAN 7, with its Lambertian surface, preserves all of the above scattered/reflected path-

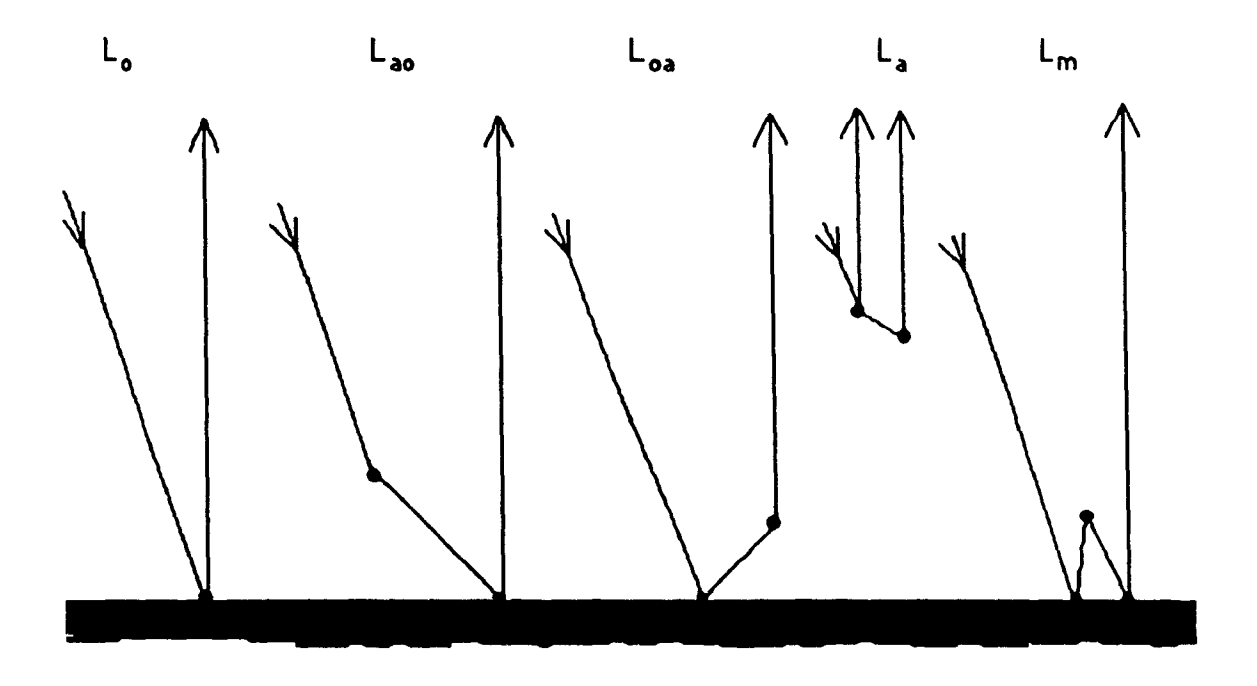


Figure 3.4. The various pathways followed by radiation contributing to the satellite measured radiance.

中はは

ways in its TOA radiance calculations. The method used in the removal and replacement of the Lambertian surface with the ocean surface model destroys some of the preserved pathways, thus introducing errors. However, these errors are minimized as described below.

The following LOWTRAN 7 products are needed:

 $L_{sat}^{Low}(\mu, \mu_0, \phi_r) = TOA$  radiance over a Lambertian surface whose albedo,  $\alpha(\mu_0)$ , is taken as a function of the SZA and set equal to  $\rho_{aw}(\mu_0)$ 

 $L_g^{Low}(\mu',\mu_o,\phi'_r) \ = \ Total \ downwelling \ radiance \ over \ a \ non-reflecting surface$ 

 $T^{Low}(\mu)$  = atmospheric transmittance from surface to space

Neglecting the ocean colour contribution for now, the flat ocean model reflects the radiation specularly, and thus, it is appropriate to write the ocean reflection function,  $R_0$ , as

$$R_o(\mu', \mu, \phi'_r) = \delta(\mu' - \mu, \phi' - \phi)\rho(\mu)$$

where  $\delta$  is the delta function.

The ocean model contribution to the TOA radiance from the surface is given by

$$\begin{split} L_g\uparrow(\mu,\mu_o,\phi_r) &= \int L_g^{Low}(\mu',\mu_o,\phi'_r) R_o(\mu',\mu,\phi'_r) \mathrm{d}\mu' \mathrm{d}\phi' \\ &= \rho(\mu) L_g^{Low}(\mu,\mu_o,\phi_r) \end{split}$$

At this point the colour contribution,  $L_{\text{C}}$  (equation 3.12) can be included. Thus the ocean model contribution to the TOA radiance is simply

$$L_{sat}^{o}(\mu, \mu_{o}, \phi_{r}) = T^{Low}(\mu) \left[ \rho(\mu) L_{g}^{Low}(\mu, \mu_{o}, \phi_{r}) + L_{c}(\mu) \right]$$
(3.13)

This perfectly preserves Lo and Lao, while including the ocean colour.

The LOWTRAN 7 Lambertian surface contribution to the TOA radiance is given by

$$L_{\text{sat}}^{\text{Lam}}(\mu, \mu_{\text{o}}) = T^{\text{Low}}(\mu) \frac{\alpha(\mu_{\text{o}})}{\pi} \int \mu' L_{\text{g}}^{\text{Lpw}}(\mu', \mu_{\text{o}}, \phi'_{\text{r}}) d\mu' d\phi'$$
(3.14)

Finally, the corrected view of the atmosphere-ocean from the TOA is simply

$$L_{sat}(\mu, \mu_0, \phi_r) = L_{sat}^{Low}(\mu, \mu_0, \phi_r) - L_{sat}^{Lam}(\mu, \mu_0) + L_{sat}^{o}(\mu, \mu_0, \phi_r)$$
(3.15)

This in effect preserves the  $L_a$  component which is part of  $L_{sat}^{Low}$ . Moreover, the  $L_{0a}$  and  $L_m$  components are approximately preserved by having  $\alpha(m_0) = \rho(m_0)$  in the calculation of  $L_{sat}^{Low}$  and  $L_{sat}^{Lam}$ . Fortunately  $L_{0a}$  and  $L_m$  are also small when compared to the magnitude of the other three contributing factors, especially at high solar elevation (because ocean reflectivity is small), so that errors are small.

To verify the model, a comparison was made to the TOA reflectance<sup>c</sup> pattern over water, under clear sky conditions, taken from Nimbus-7 ERB

<sup>&</sup>lt;sup>e</sup>Reflectance is herein defined as the radiance normalized by  $\mu_0 F_0/\pi$ , where  $F_0$  is the solar irradiance measured at the top of the atmosphere.

(Taylor and Stowe, 1984). An absolute comparison was impossible since Nimbus-7 measurements were broad-band (0.2 - 4.5  $\mu$ m), and the published results were averaged over SZA bins. A relative comparison, however, was possible. Since it is an angular TOA reflectance pattern that is being compared, a narrow-band reflectance which shows the same angular dependance as that of the broad-band reflectance is all that is needed to solve the band-width difference problem. Figure 3.5 depicts similarities between the angular variation of the 0.86 µm radiance and the broadband radiance using LOWTRAN 7 simulations (Lambertian surface). A typical result comparing the TOA reflectances is shown in Figure 3.6. The backward scatter direction is RAZ = 0°. To alleviate the broad-to-narrow band radiance conversion problem, the reflectance was normalized to each of the results' respective 90° RAZ. The 90° RAZ was chosen as it shows the least variability of reflectance when compared to the other relative azimuth angles, because of its minimum in the scattering phase function. In simulation, the reflectance was not averaged throughout the SZA bin because the weighting of each Nimbus-7 measurement within the bin was not known. Instead, the SZAs used in simulation were the SZA bounds of the bin. As shown in Figure 3.6 the Nimbus-7 measurements do, in fact, lie within these bounds in the forward-scatter direction and very close to, or within, these bounds for the back-scatter direction. Thus model results compared to Nimbus-7 measurements are quite good considering that the comparison was made for a flat ocean model whereas in the real world, surface waves exist.

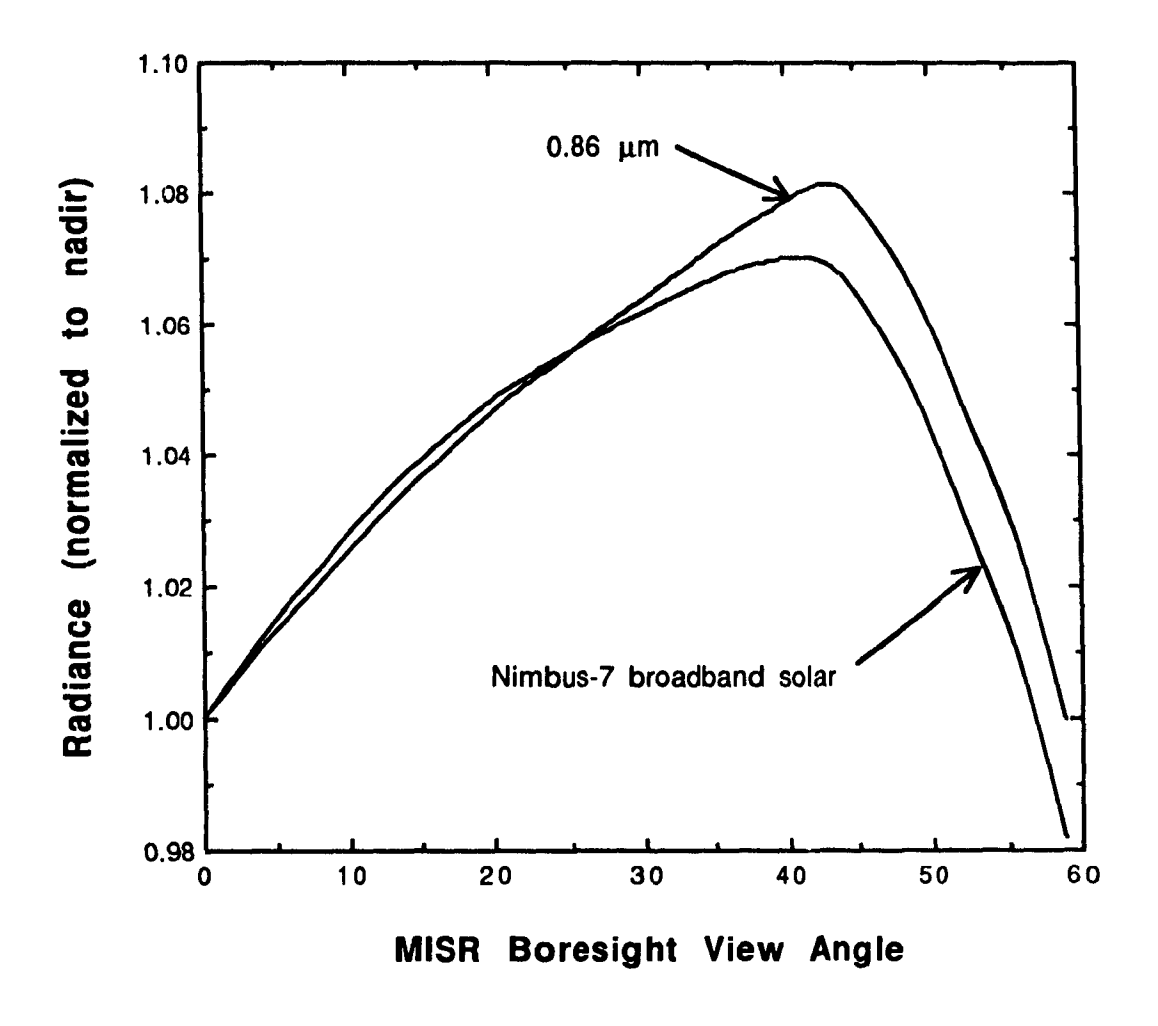


Figure 3.5. LOWTRAN 7 simulations of TOA radiance showing the similarity in angular variation between the 0.86  $\mu$ m radiance and the broadband (0.2  $\mu$ m - 4.5  $\mu$ m) radiance. (Tropical Atmosphere; Lambertian Surface, Overhead Sun)

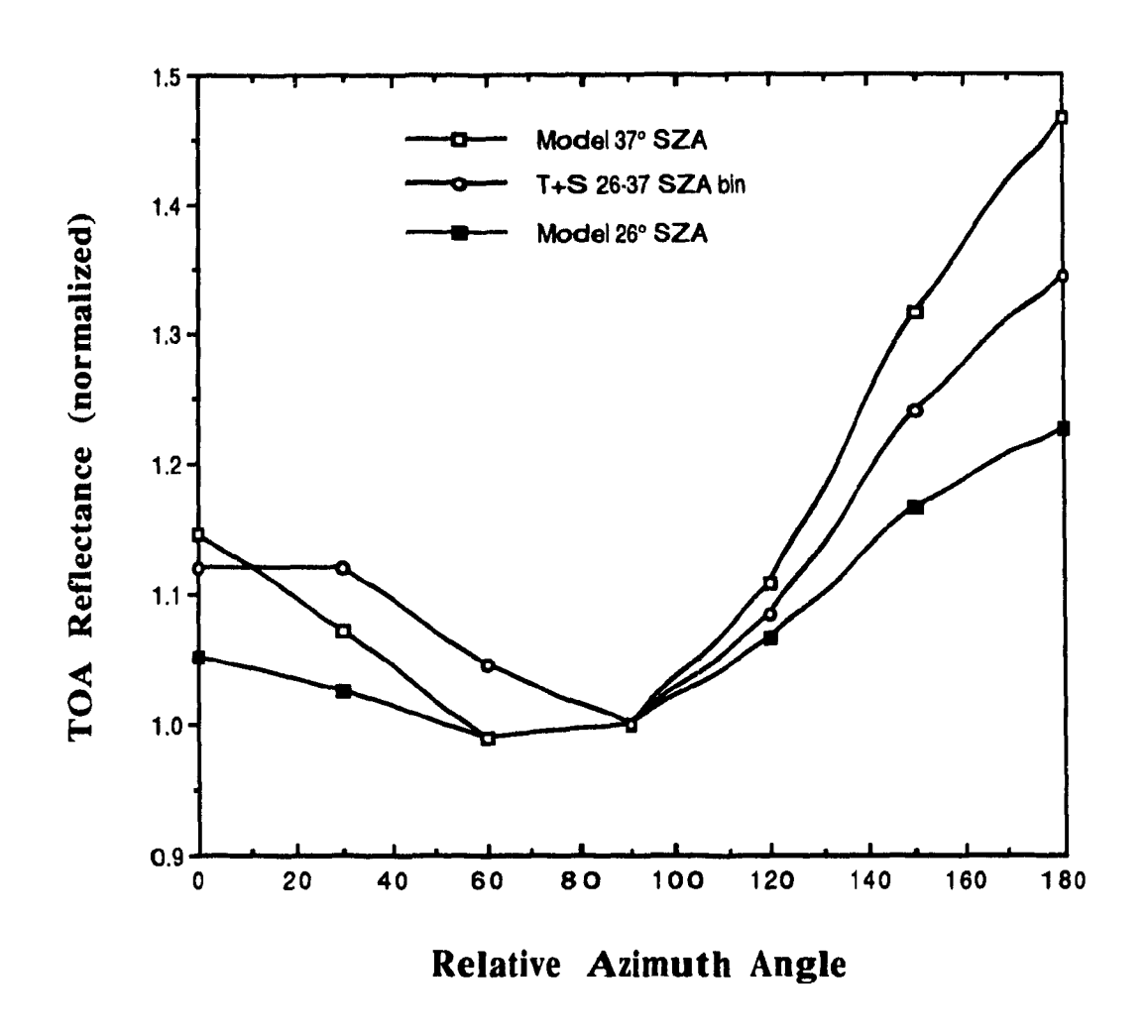


Figure 3.6. Comparison of TOA reflectance pattern over clear sky-ocean of atmosphere-ocean model simulations to Taylor and Stowe (1984). The view angle is 70.5° (MISR-D camera), and the solar zenith angle ranges from 26° to 37°.

# 3.2.4. The Predetermined Clear Sky Threshold Technique

As discussed in Chapter 2, all conventional cloud detection algorithms apply some type of threshold to discriminate between cloud and no-cloud pixels. However, many of these algorithms work poorly in detecting cirrus clouds. This section and the next develop a new approach to cirrus cloud detection. This section describes the Predetermined Clear Sky Threshold (PCST) technique which identifies clear sky pixels, while Section 3.2.5 describes an approach using the Band-Differenced Angular Signature (BDAS) of the scene. The BDAS technique takes those pixels that were not retrieved as clear sky using the PCST and identifies them as high-level or low-level clouds. Since this approach requires multi-angle views, the PCST and BDAS will be calculated for the MISR instrument.

Many existing cloud detection algorithms can be applied to MISR data; most of these require other data sources (such as temperature and humidity profiles). However, it would be convenient if other data sources were not necessary, leaving the possibility for real-time cloud detection. In order to do so, a Clear Sky Maximum Reflectance (CSMR) approach was used to derive the PCST. This approach takes into account the maximum contribution to the satellite-measured reflectance from the ocean surface, atmospheric gases, and atmospheric aerosols. The maximum possible reflectance under clear sky conditions defines the threshold. Because of the bidirectional reflectance of the ocean, the Rayleigh phase function of the atmospheric gases, and the scattering phase function of the aerosols, the threshold will depend on the viewing/solar geometry.

Figure 3.7 shows the rate of increase in reflectance from nadir to oblique views. The rate of increase is greater for the presence of cirrus clouds than it is under clear skies alone. Thus the most oblique view (MISR-D camera) should be used for thresholding since it offers the greatest sensitivity in discriminating cloud vs. no-cloud. The MISR 0.86 um channel was chosen for the CSMR approach because it is less sensitive to changes in atmospheric and oceanic constituents, compared to the other MISR channels. For example, the 0.86 µm channel lies outside the Chappuis bands of ozone and the 0.72-µm water vapor band (Goody, 1964). The aerosol effect is also larger at shorter wavelengths. The effects of sediments, phytoplankton, and yellow substance, as well as the clear water contribution (which all give rise to ocean colour) are much smaller at 0.86 µm as compared to the shorter MISR wavelengths (Figure 3.3). In fact ocean colour contribution at 0.86 µm is small enough that the upwelling contribution from below sea surface can be considered zero (R = 0).

LOWTRAN 7 carries six different atmospheric profiles taken from NASA (1976) and NASA (1966). These range from tropical to sub-arctic winter conditions. The profile giving rise to the largest TOA reflectance values was the sub-arctic winter due to its low water vapor concentration (thus low water vapor continua absorption) relative to other profiles; hence, it was used in the CSMR approach. In the case of aerosols, LOWTRAN 7 uses an empirical relationship between maritime aerosol concentration and wind speed (Kneizys et al., 1983). To avoid problems with white caps, the maximum wind value was taken to be 15 m/s (Payne,

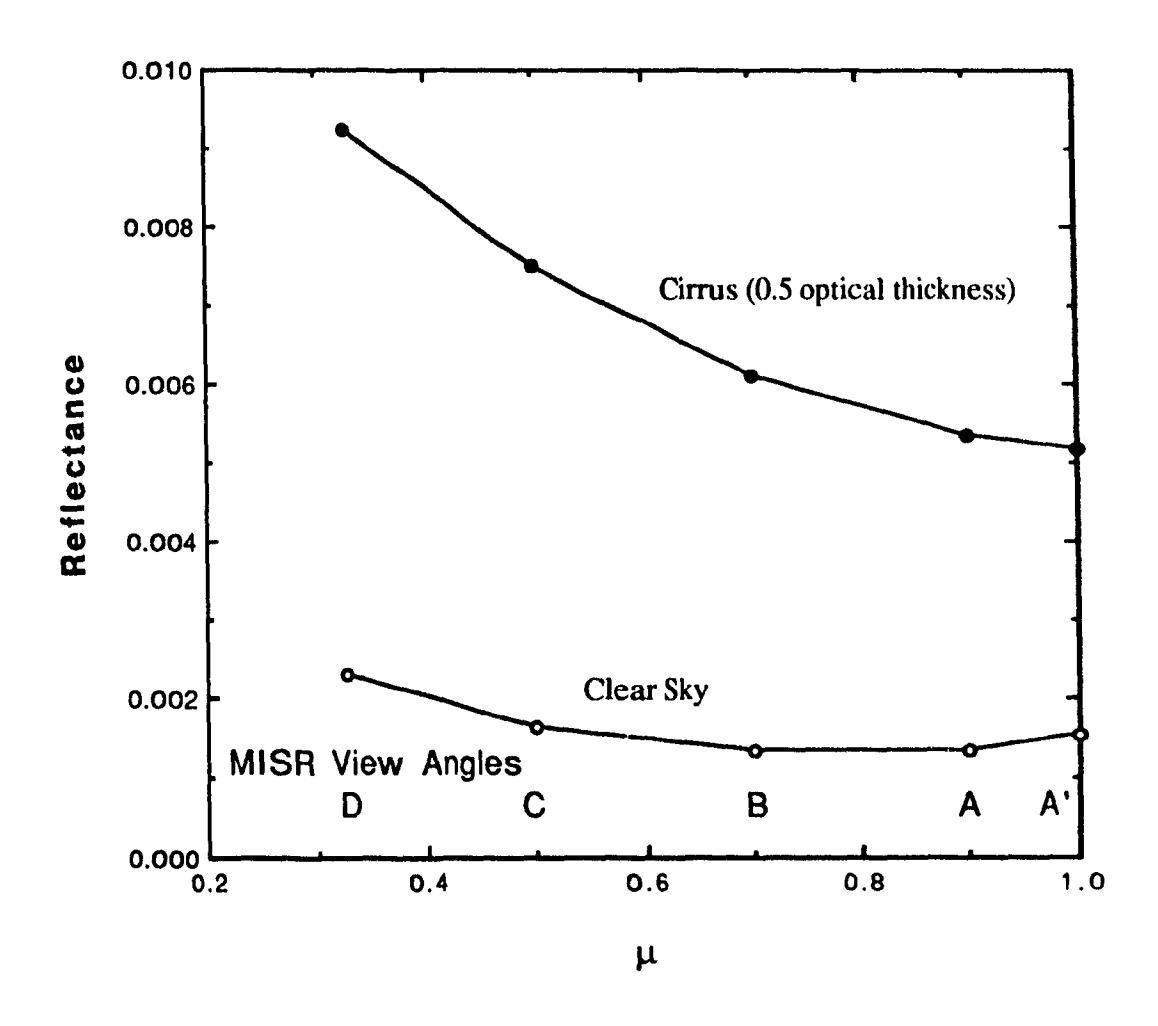


Figure 3.7. LOWTRAN 7 simulations of TOA 0.86 µm radiances. (tropical atmosphere; black surface; cirrus cloud top and bottom height = 12 km and 11 km, respectively; aerosol concentration set by 5 m/s winds; overhead sun)

1972). Continental aerosols blown over the ocean is also taken into account by LOWTRAN 7. However, light concentrations were assumed.

Work by Preisendorfer and Mobley (1986) has shown that maximum reflectance is highest for flat ocean except in the mid-solar zenith angle range where the effects of surface roughness can increase the ocean reflectance slightly, depending on the wind speed and relative azimuth angle between sun and wind direction. This increase was small enough to ignore. Thus the flat ocean model of Section 3.2.2 was used in the calculations of the PCST.

The above extremum in atmospheric and oceanic state sets the threshold, that is the maximum reflectance the MISR-D camera is expected to observe under clear sky conditions. The minimum detectable optical thickness of a cirrus cloud will give rise to reflectances greater than these PCSTs. Thus, with no a priori knowledge of atmospheric and oceanic state, the conditions giving rise to minimum reflectance (i.e. worst case scenario) are now assumed to determine the minimum detectable cirrus cloud optical thickness. These conditions correspond to the subvisual cirrus profile (Shettle et al., 1988), high clouds, and the tropical atmospheric profile under light aerosol concentrations. Under a diffuse sky illumination, the reflectance of the ocean decreases about 1% with an increasing wind speed from 0-15 m/s, and depends on the type of sky illumination (Preisendorfer and Mobley, 1986). Thus for diffuse radiation, the flat ocean case is a good assumption for the minimum reflectance state. However a direct component is still present below the thin cloud. The flat ocean case is a poor model for minimum reflectance of the direct component at low solar elevations (SZA > 60°). At these angles the effect of surface roughness reduces the reflectance greatly and the reflection function becomes difficult to predict. Despite this shortcoming, the flat ocean model was used in the minimum reflectance calculations of a cloudy atmosphere because of its great simplicity as compared to a rough ocean surface model. Note that this does not effect the PCST; instead, it will slightly increase the value of the minimum detectable cloud optical thickness.

From the MISR design, the fore and aft cameras have a relative azimuth angle difference of 180°. The simulations have found that in applying the PCST the camera (fore or aft) whose relative azimuth angle with the sun is between 90° and 180° (that is the side which picks up more of the forward scattering) should be used in the detection of cirrus clouds over ocean. The MISR-D camera should be used for the detection except where sun glint is encountered, in which case the MISR-B camera can be substituted (over the MISR-C camera which may also be contaminated by sun glint).

With this rule, Figures 3.8 (a) - (d) compare a cirrus cloud of visual (0.55 µm) optical thickness of 0.5 against the clear sky threshold for various relative azimuth angles. The figures show that this cloud is detectable even when a 3% uncertainty in instrument measurement is included. This is better than other global cloud detection algorithms such as Rossow and Lacis (1990) who consider clouds to exist only if the retrieved cloud optical thickness > 1.2. Keep in mind that the results presented here are comparing extreme scenarios between the clear sky and cloudy atmospheres. If any a priori knowledge of atmospheric aerosol concentration and/or wind speeds, temperature, etc., is known, then

threshold values would in most cases decrease, further improving the ability to detect thinner clouds. Of course, this technique still shares some inherent problems of other algorithms, mainly the misclassification of surface reflectance anomalies (e.g. fog, white caps, ocean foam) for cloud. However when this technique is used in concert with the Band-Differenced Angular Signature technique described below, the problem of misclassification is greatly reduced.

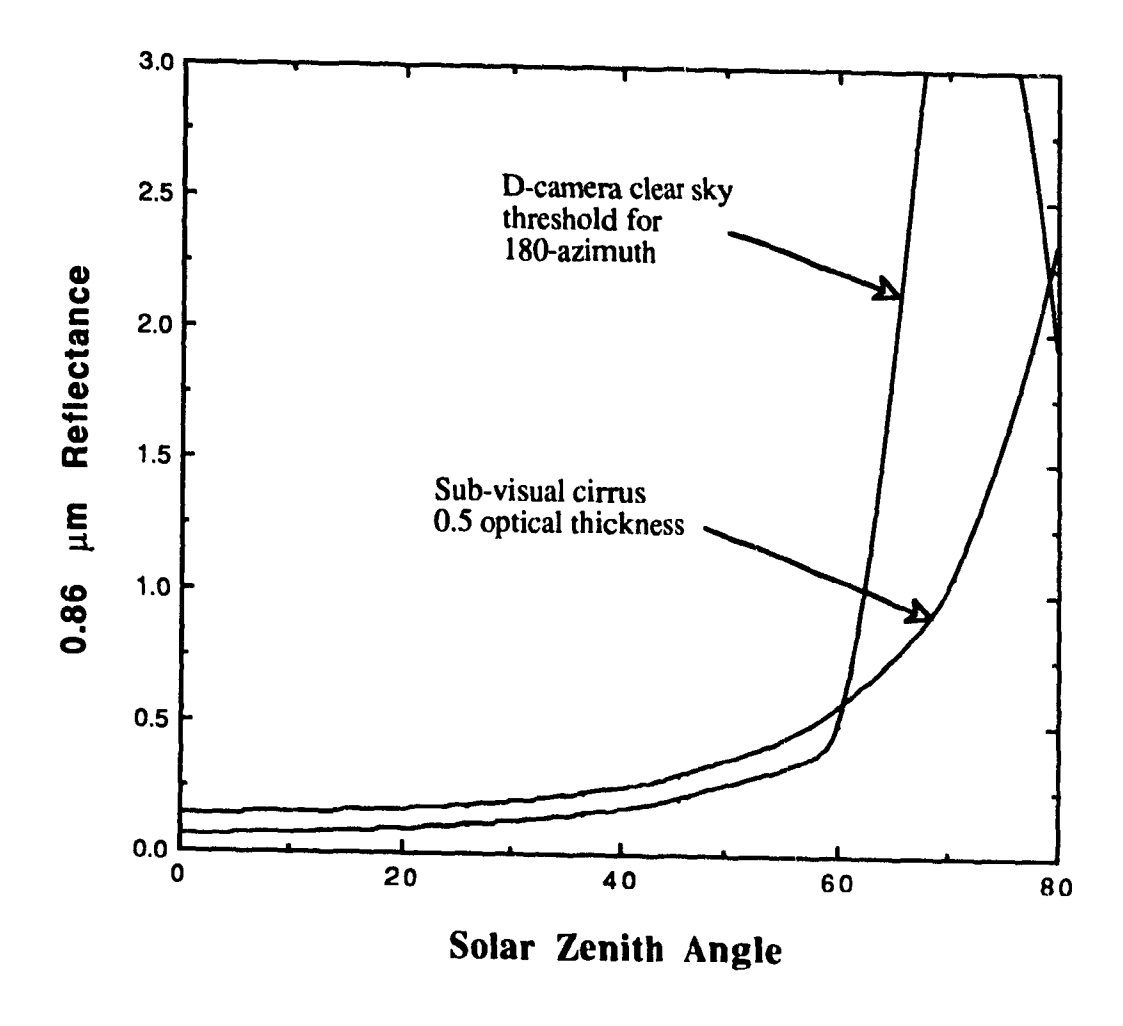


Figure 3.8 (a). Comparison of thin cirrus cloud (base height = 11 km, thickness = 1 km) with the predetermined clear sky threshold calculated for the MISR-D camera with a RAZ =  $180^{\circ}$ .

Figure 3.8 (b). Comparison of thin cirrus cloud (base height = 11km, thickness = 1 km) with the predetermined clear sky threshold calculated for the MISR-B camera with a RAZ = 180°.

Figure 3.8 (c). Comparison of thin cirrus cloud (base height = 11 km, thickness = 1 km) with the predetermined clear sky threshold calculated for the MISR-D camera with a RAZ =  $150^{\circ}$ .

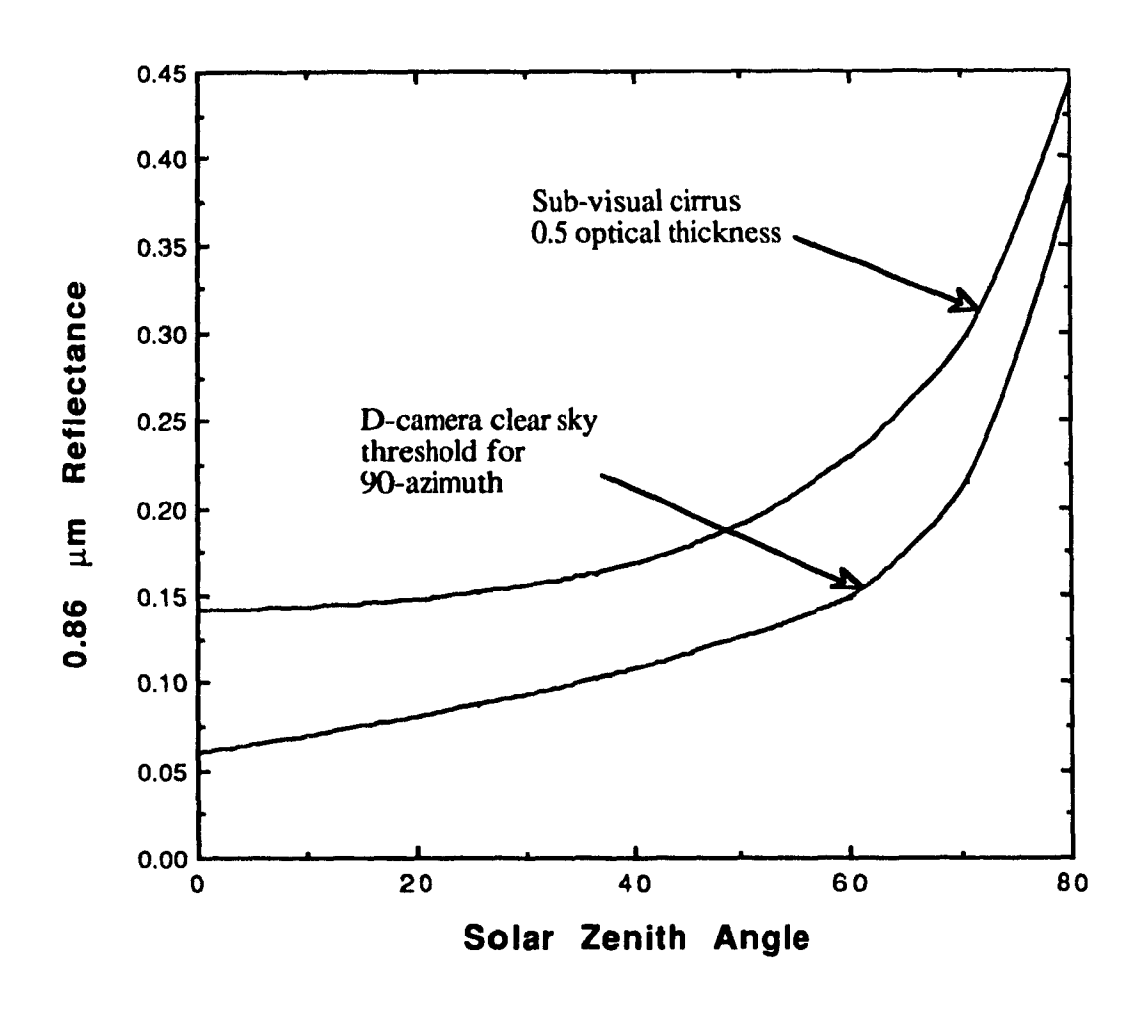


Figure 3.8 (d). Comparison of thin cirrus cloud (base height = 11 km, thickness = 1 km) with the predetermined clear sky threshold calculated for the MISR-D camera with a RAZ =  $90^{\circ}$ .

#### 3.2.5. The Band-Differenced Angular Signature Technique

For many years, scientists have identified atmospheric constituents by observation of their spectral signature. In the past two decades multispectral approaches have gained popularity in cloud detection. This section describes a new approach which combines the spectral signature with its angular variation, to give the Band-Differenced Angular Signature (BDAS) of the scene. This new approach takes the difference between two solar spectral reflectances as a function of view angle. The resulting angular signature is used to discriminate between low-level and high-level clouds, as well as surface reflectance anomalies. The MISR instrument is ideal for the application of this new technique. MISR's 0.86 µm reflectance is subtracted from the 0.44 µm reflectance. Because a factor of 16 exists between their respective Rayleigh scattering cross-sections (which is the largest difference between all MISR spectral channels), different Rayleigh scattering contributions are expected. The magnitude of this difference will not be the same between clear and cloudy skies. This is because the cloud masks a large part of the Rayleigh atmosphere from the satellite. Higher clouds will have a larger masking effect compared to lower clouds. The same is true for thicker clouds. Thus, the BDAS of high thick cirrus clouds is expected to be very different from lower level clouds or from clear skies. This section focuses on detecting cirrus clouds based on the BDAS pattern alone (i.e. not on the absolute value of the BDAS or radiance measurement). Inclusion of, say, the absolute value of the BDAS would require further modelling, and would certainly improve the detection and classification scheme. The planning for this approach is already in its preliminary stage.

LOWTRAN 7 coupled with the flat ocean model was used for the BDAS simulations. Since the ocean colour contribution and its angular variation with sea surface state is small, the flat ocean assumption introduces little error to the BDAS. The 0.44  $\mu$ m ocean colour contribution was set at a reflectance R = 0.03 (a typical value). The Q = 5 assumption (equation 3.12) is fine for nadir measurements (Austin, 1980) but uncertain for oblique views. However, it was more important to get accurate calculations for the nadir views because the ocean colour contribution to nadir-satellite-measured radiance is much more significant than at oblique views. Even so, the colour contribution to the TOA reflectance is small (e.g. max. of 8% at nadir for a clear ocean of R=0.07 @ 0.44  $\mu$ m).

In the BDAS simulations the same atmospheric profile was used for both clear and cloudy skies. LOWTRAN 7's tropical atmosphere under light aerosol concentrations was used because it offered minimum TOA band-differenced radiance contribution, thus simulating the worst possible case in using the BDAS for cloud discrimination. The same 0.5 optically thick cirrus cloud detectable by the predetermined thresholds, as well as other cloud forms, was used in the BDAS simulations. All viewing/solar geometries have been examined with the typical results shown in Figures 3.9 - 3.14. Figures 3.9 and 3.10 show the BDAS typical of all sun/viewing geometries, with the exceptions shown in the other four figures. In these figures, the negative view angles are picking up the forward scatter. Figure 3.9 shows that clear sky and surface fogs both have a "bowl" shaped BDAS. Thus from their BDAS pattern alone, clear

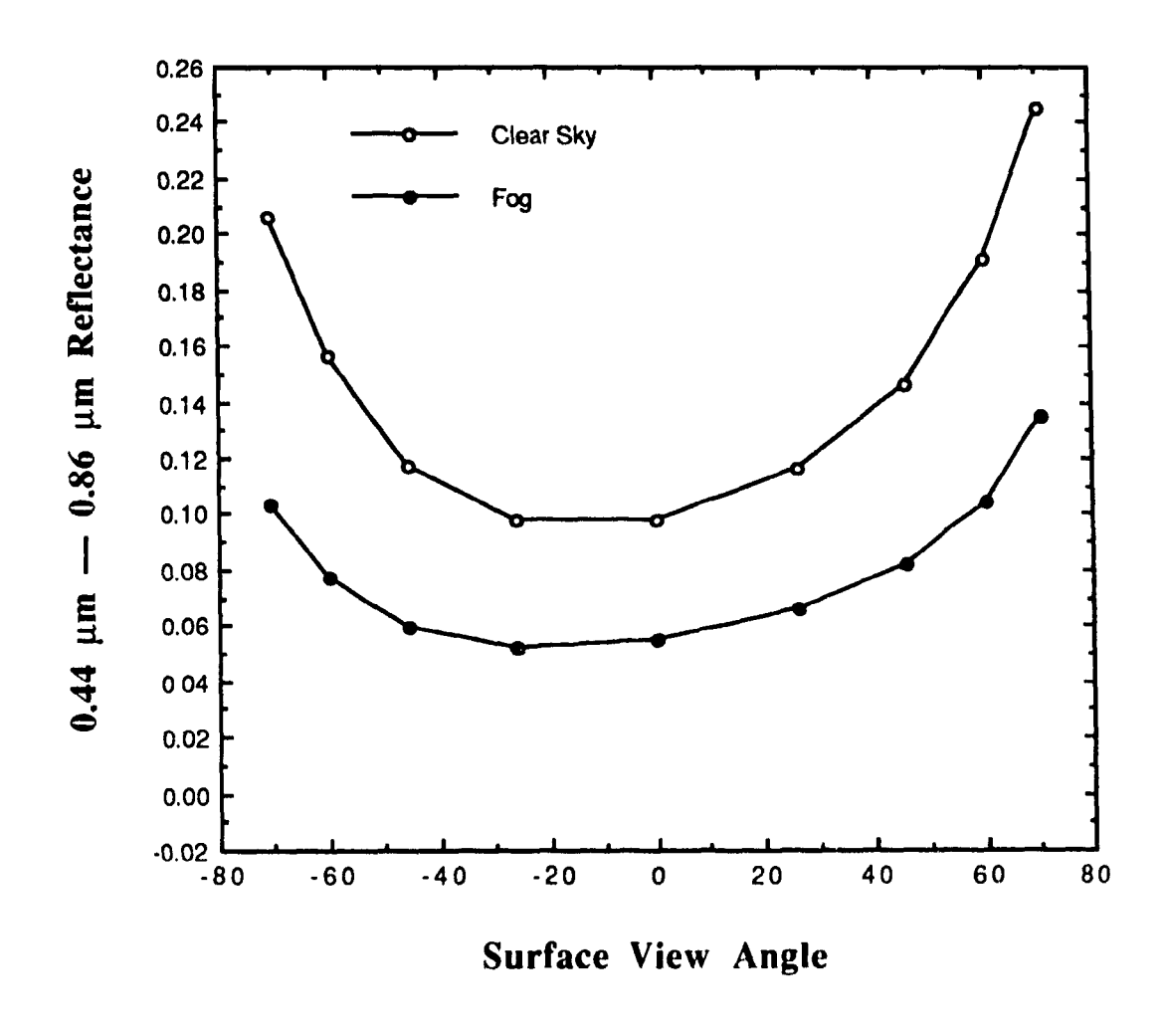


Figure 3.9. Band-Differenced Angular Signatures for a SZA =  $60^{\circ}$  and a RAZ =  $60^{\circ}/120^{\circ}$ . The atmospheric/oceanic details are in the text.

- Clear sky
- Fog: Type = radiation (Kneizys et al., 1980), surface range = 2 km.

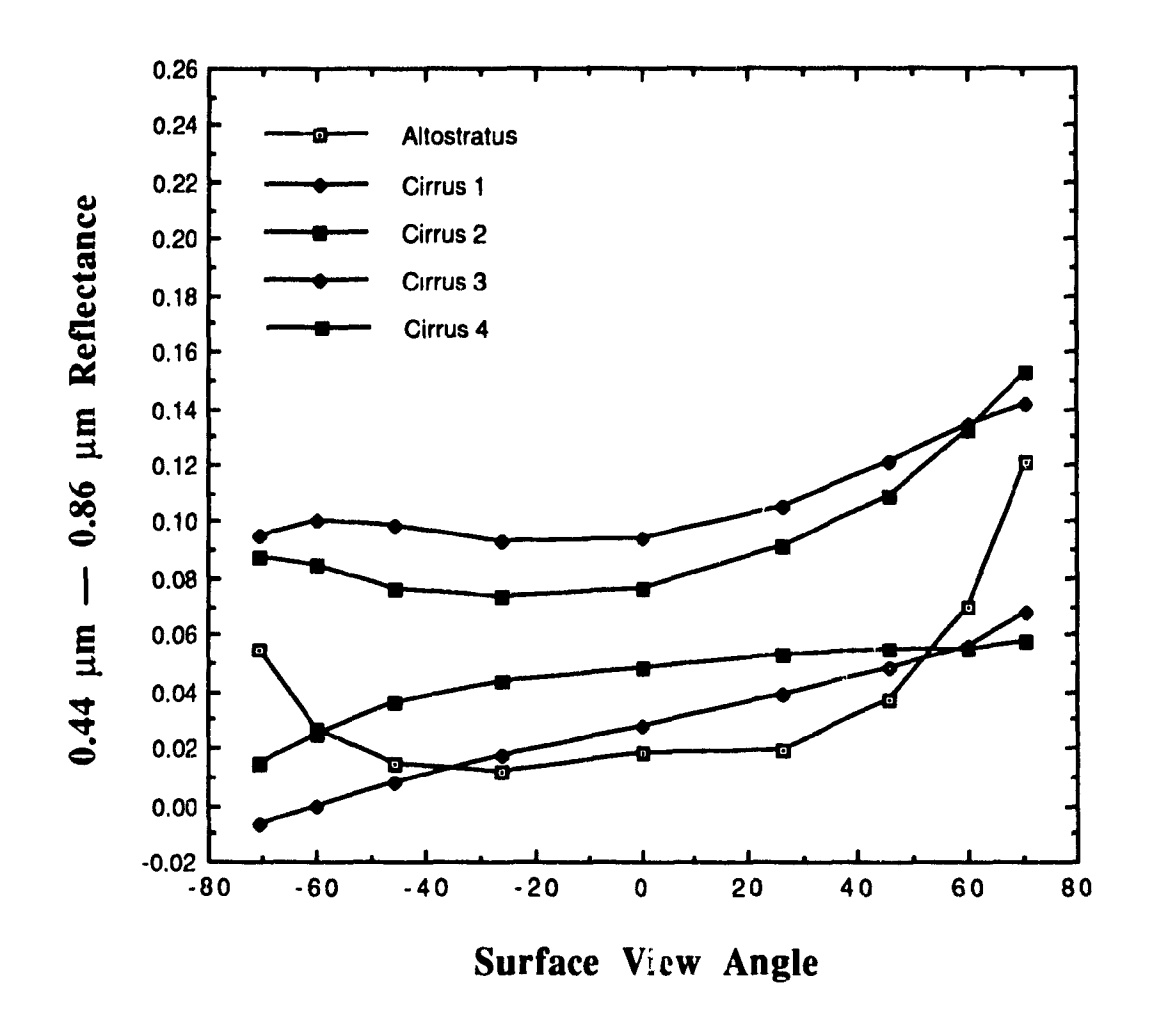


Figure 3.10. Band-Differenced Angular Signatures for a SZA =  $60^{\circ}$  and a RAZ =  $60^{\circ}/120^{\circ}$ . The atmospheric/oceanic details are in the text.

Cloud models from Shettle et al., 1988.

- Altostratus: Base = 2.4 km; top = 3 km; optical thickness = 54.5
- Cirrus 1: Base = 11 km; top = 12 km; optical thickness = 0.5; type = Subvisual
- Cirrus 2: Base = 5 km; top = 6 km; optical thickness = 0.5; type Subvisual
- Cirrus 3: Base = 5 km; top = 6 km; optical thickness = 10; type = Cirrus Profile
- Cirrus 4: Base = 11km; top = 12 km; optical thickness = 10; type = Cirrus Profile

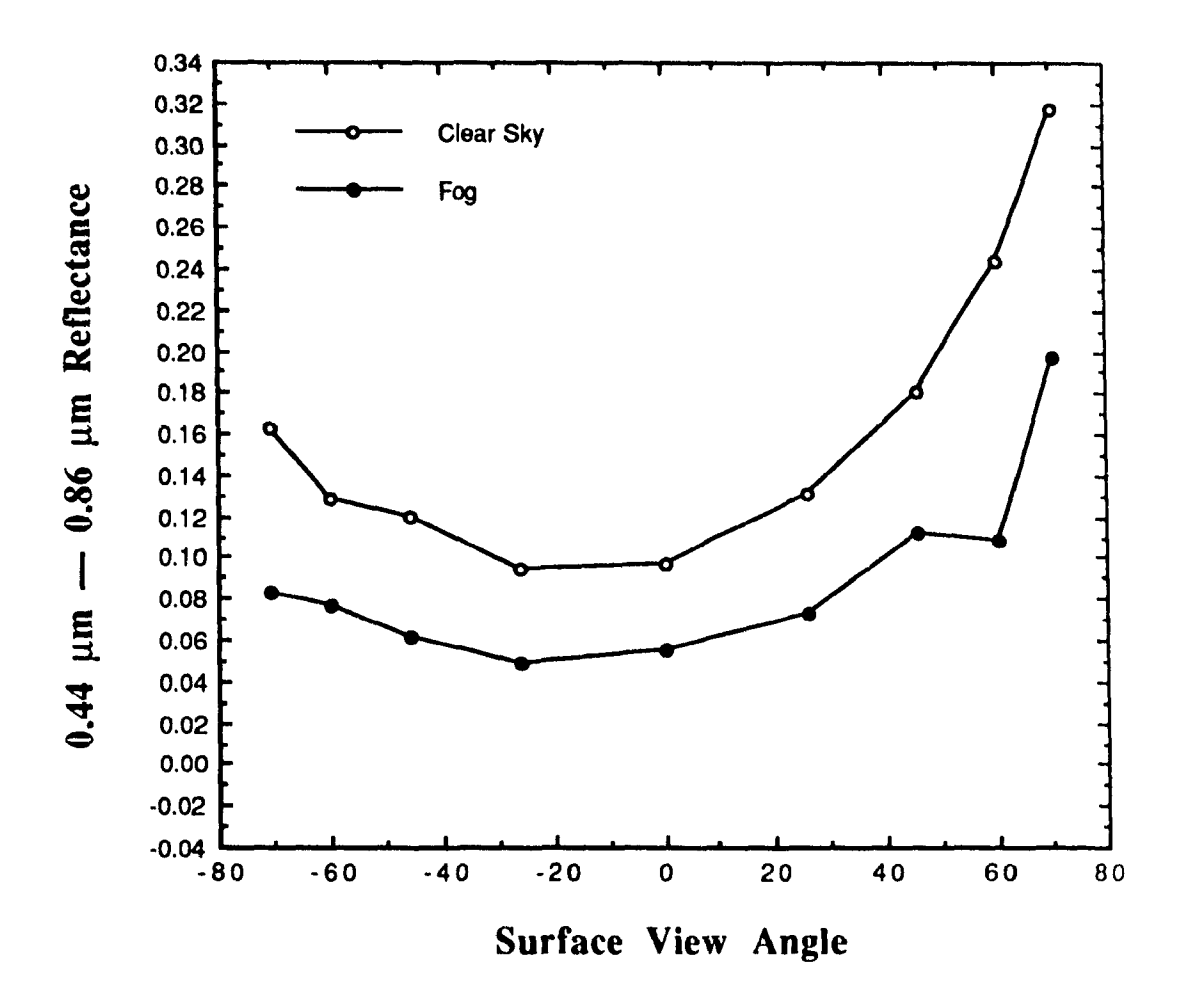


Figure 3.11. Band-Differenced Angular Signatures for a SZA =  $60^{\circ}$  and a RAZ =  $0^{\circ}/180^{\circ}$ . The atmospheric/oceanic details are in the text.

- Clear sky
- Fog: Type = radiation (Kneizys et al., 1980), surface range = 2 km.

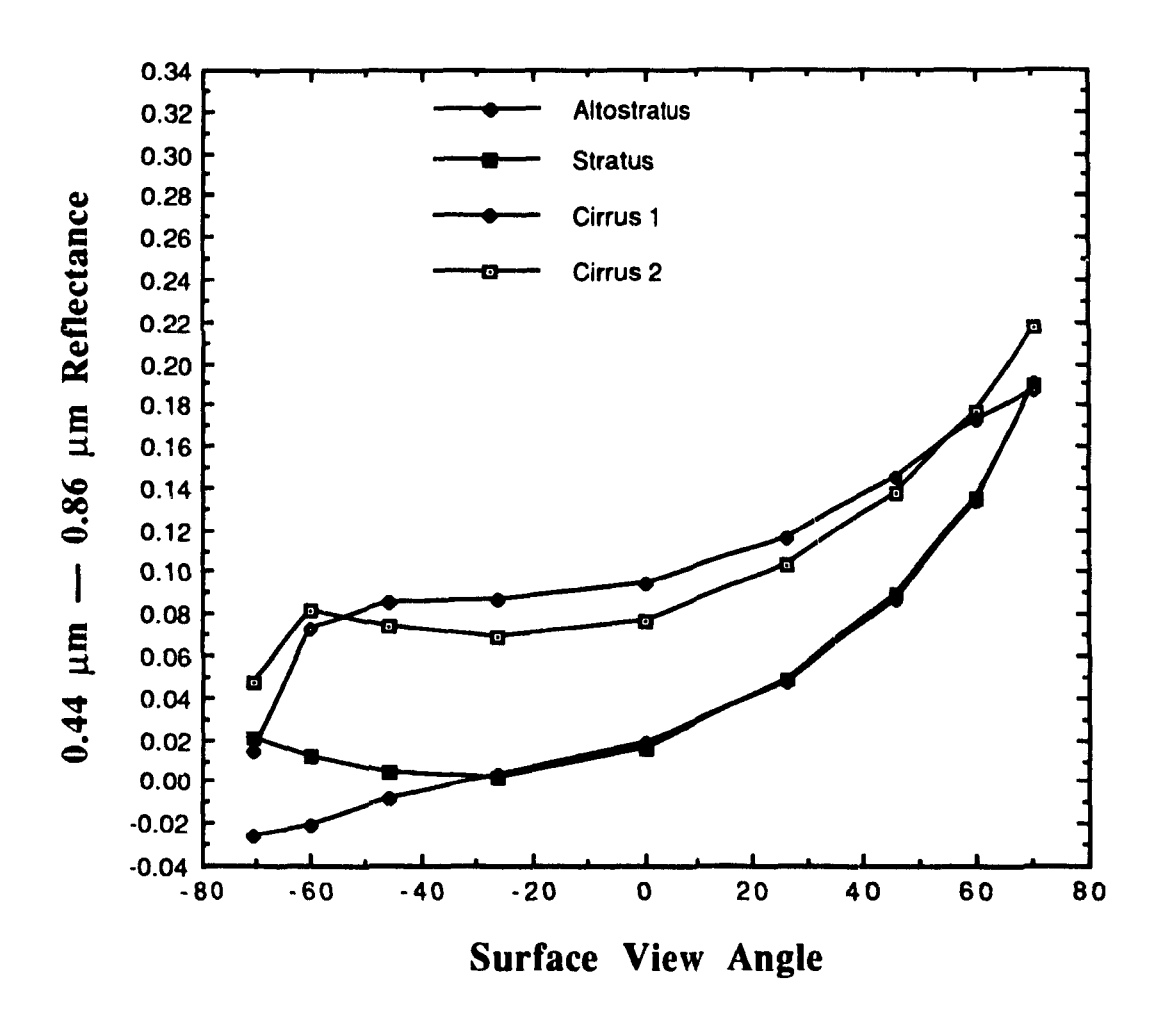


Figure 3.12. Band-Differenced Angular Signatures for a SZA =  $60^{\circ}$  and a RAZ =  $0^{\circ}$ . The atmospheric/oceanic details are in the text.

Cloud models from Shettle et al., 1988.

- Altostratus: Base = 2.4 km; top = 3 km; optical thickness = 54.5
- Stratus: Base = 0.33 km; top = 1 km; optical thickness = 37
- Cirrus 1: Base = 11 km; top = 12 km; optical thickness = 0.5; type = Subvisual
- Cirrus 2: Base = 5 km; top = 6 km; optical thickness = 0.5; type Subvisual

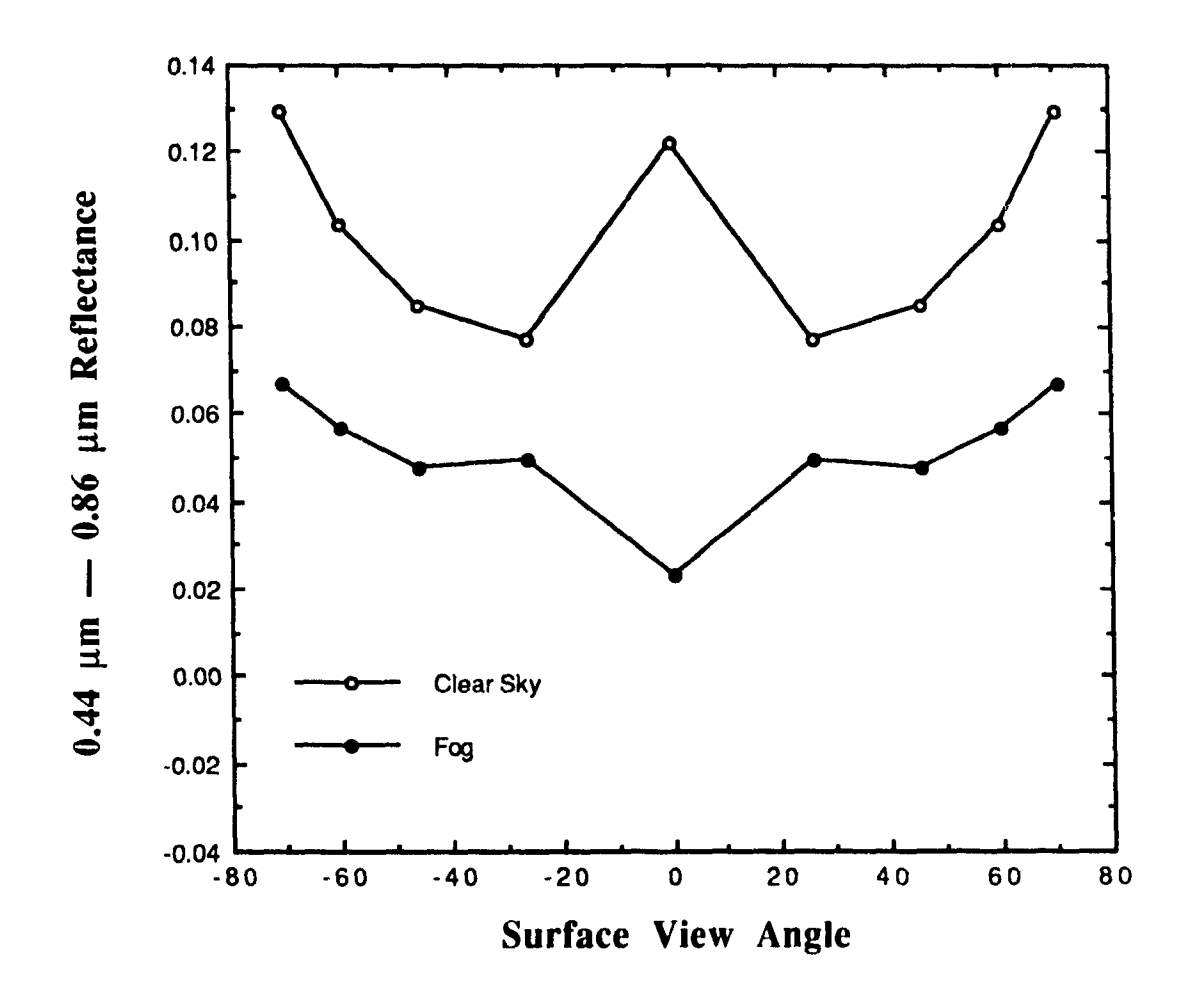


Figure 3.13. Band-Differenced Angular Signatures for a SZA =  $0^{\circ}$ . The atmospheric/oceanic details are in the text.

- Clear sky
- Fog: Type = radiation (Kneizys et al., 1980), surface range = 2 km.

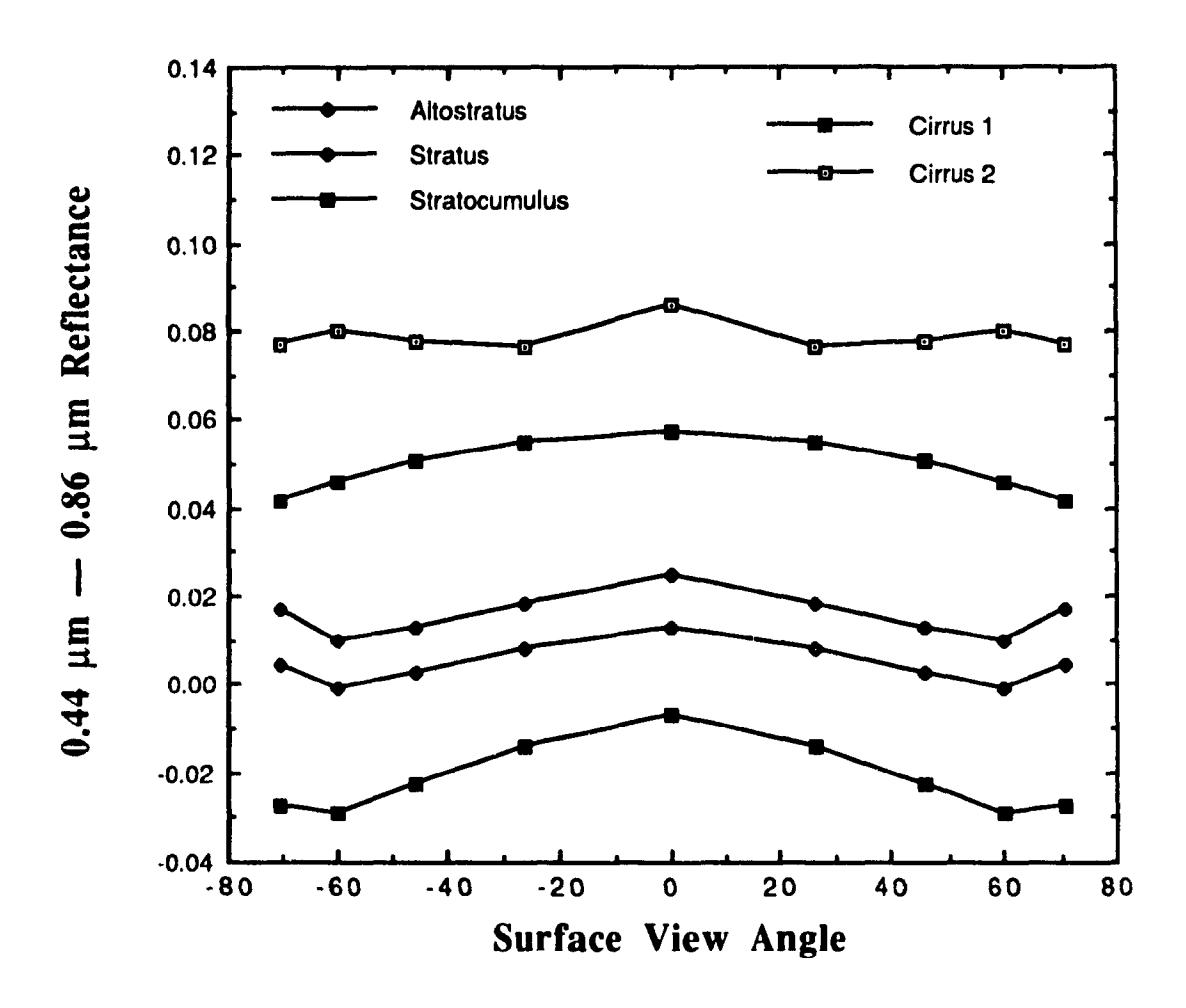


Figure 3.14. Band-Differenced Angular Signatures for a SZA = 0°. The atmospheric/oceanic details are in the text.

Cloud models from Shettle et al., 1988.

- Altostratus: Base = 2.4 km; top = 3 km; optical thickness = 54.5
- Stratus: Base = 0.33 km; top = 1 km; optical thickness = 37
- Stratocumulus: Base = 0.66 km; top = 2 km; optical thickness = 47.8
- Cirrus 1: Base = 5 km; top = 6 km; optical thickness = 10; type = Cirrus Profile
- Cirrus 2: Base = 11 km; top = 12 km; optical thickness = 0.5; type = Subvisual

sky and fog cannot be discriminated. Figure 3.10 shows the BDAS for 5 different clouds. The lowest cirrus cloud used was 5 km in cloud base altitude which is consistent with the 0°C isotherm of LOWTRAN 7's tropical atmosphere. This is also consistent with the lowest observed cirrus with a cloud center altitude of 4 km measured at mid-latitudes (Dowling and Radke, 1990). Unlike clear/foggy skies, a distinct feature of cirrus clouds is the decrease in band difference reflectance with increasing viewing obliquity in the forward-scatter direction (surface view angle < 0). As Figure 3.10 shows, this feature is more pronounced with increasing cloud height and optical thickness. For the lowest thin cirrus, the band-differenced reflectance increases slightly with viewing obliquity. This increase is much more gradual than that of clear/foggy skies. In fact, when instrument noise (which is always less than 0.01 in the band-differenced reflectance) is added, the sign of the gradual slope is uncertain. Figure 3.10 also shows an altostratus cloud with a cloud top height of 3 km. Here the cloud is low enough to pick up the "bowl" like pattern of the clear/foggy sky BDAS shown in Figure 3.9; thus, it cannot be discriminated against clear sky based on the BDAS pattern alone.

An example of when clear sky, fog, and low-level clouds can be discriminated is when the measurements are made along the sun/viewing plane (i.e. a relative azimuth angle of 0°/180°). Figure 3.11 and 3.12 show the results for a SZA = 60°. The clear sky BDAS pattern remains the same as in Figure 3.9. Fogs exhibit a "notch" in their BDAS "bowl" shape in the back-scatter direction at a view angle equal to the SZA. This is because the small end of the droplet size spectrum of the fog (Kneizys et al., 1983) greatly effects the scattering efficiency factor. When aver-

aged over the size parameter distribution at constant wavelength, the scattering efficiency factor is found to be greater at 0.86 µm than it is at 0.44 µm. Figure 3.12 also shows the altostratus cloud taking on the same shape of the cirrus BDAS. Here, the cirrus and altostratus may be discriminated by comparing the slopes in band-differenced reflectance of the most oblique forward-view angles; however, due to the uncertainty in MISR measurements, a threshold in the BDAS slope has not been set.

Figures 3.13 and 3.14 represent the overhead sun scenario. In this case, the fog still has its "notch". For overhead sun, the SZA is now small enough that the band-differenced specular peak reflectance now shows up in the clear sky BDAS. In Figure 3.14 the clouds have the same BDAS as before except that it's now symmetrical about nadir; however, the noise level is large enough that cloud type cannot be discriminated based on the relative BDAS alone.

The BDAS results of Figures 3.9-3.14 are summarized in Table 3.2 and take into account all view/sun geometries. The summary uses a quantitative approach and is based on the BDAS pattern alone.

The largest uncertainty in the results probably lies in the LOWTRAN 7 cirrus cloud model. The cirrus ice particles used in LOWTRAN 7 are spherical rather than cylindrical or platelets. Takano and Liou (1989b) point out that the spherical assumption "... is inadequate for use in the interpretation of bidirectional reflectance from cirrus clouds". Fortunately it is not the absolute bidirectional reflectance that is being used here but instead the band-differenced bidirectional reflectance. The errors brought about when using the spherical assumption over, say, the hexagonal assumption are in the relative change of extinction cross-section, from 0.44

Table 3.2. A summary of the BDAS results

View/Sun Geometry	View¹ Range	Condition <sup>2,3</sup>	Results
SZA >10°, 10°< RAZ <170°	∀θ	∂I/∂θ > <b>0</b>	cirrus
	 	otherwise	unclassified
SZA >10°,  RAZ ≈0°/180°	θ < -60°	∂1/∂0 ≈ 0	low cloud
		91/96 >> 0	cirrus
SZA  > 0°	θ ≈ 0°	91/99  >> 0	clear/fog
		otherwise	cloud(type
			unclassified)

<sup>&</sup>lt;sup>1</sup> Surface View Angle as defined in Table 3.1

<sup>21</sup> refers to the band-differenced reflectance

<sup>&</sup>lt;sup>3</sup> Includes the effect of instrument noise

μm to 0.86 μm, between the two shapes. From Takano and Liou (1989a) this error is largest when comparing hexagonal crystals that have the same diameter-to-length ratio. Their results gave the extinction crosssection,  $C_e$ , at 0.55  $\mu m$  and 2.2  $\mu m$ . Based on the results of Shettle et al. (1988), a linear regression between Ce and wavelength is valid for wavelengths less than 2.2 µm, thus enabling errors to be estimated at  $0.44~\mu m$  and  $0.86~\mu m$ . The result is a 1.5% increase from  $C_e(0.44\mu m)$  to Ce(0.86μm) for the spherical particle and no increase for re hexagonal particle. From this, the uncertainty in the use of spherical ice particles over hexagonal ice particles in the BDAS calculations is expected to be small for the cirrus cloud contribution to the total band-differenced reflectance. However, in Takano and Liou's (1989a) work, the same ice crystal size was used, chosen from the mean size observed in cirrus ice crystal distributions. For small ice crystals at the tail end of the distribution, the scattering efficiency factor varies more rapidly as a function of wavelength. Thus for cirrus clouds containing a large amount of small ice crystals, the uncertainty in using the spherical assumption in deriving the band-differenced reflectance is expected to be higher.

## 3.3. Discussion

This chapter has dealt with the development of a new cirrus cloud detection algorithm using a multi-angle viewing instrument such as the Multi-angle Imaging SpectroRadiometer (MISR) described in section 3.1. The application of the Predetermined Clear Sky Threshold (PCST) acts as a simple discriminator for clear sky pixels. However, as in other thresholding algorithms, the PCST is plagued with the possibilities of misclassification. In this study, misclassification was reduced by coupling the PCST with a Band-Differenced Angular Signature (BDAS) technique. The BDAS technique relaxes the accuracy needed of the PCST. For example, in using the Clear Sky Maximum Reflectance (CSMR) approach to determine the PCST, the concentration of continental aerosols was light. However, coastal regions may well have a high concentration of continental aerosols. In this case the PCST may classify this region as non-clear but the BDAS will not classify this region as high cloud. Thus, it will remain as haze/fog/low-clouds or some other reflectance anomaly, unless measurements are made along the sun/viewing plane, in which case the fog, low cloud, and clear sky can be discriminated.

The sensitivity of this algorithm was measured by determining the minimum detectable cirrus cloud optical thickness. The algorithm was able to detect thin cirrus clouds of visible optical thickness as low as 0.5. This is superior to conventional global cloud detection algorithms which typically cannot detect clouds thinner than a visible optical thickness of 1. Of course other techniques using specific satellite data are available which can detect very thin clouds of less than 0.1 visible optical thick-

ness. Unfortunately these do not offer continuous global coverage over a short time scale (less than 10 days), require other data sources as input, or offer very poor spatial resolution (Chapter 2).

The PCST/BDAS algorithm requires data from one instrument only, namely MISR. Unlike other cloud detection algorithms, this algorithm requires no other data set concerning the atmospheric and oceanic state (i.e. temperature and humidity profiles, etc.) This additional knowledge, however, could be incorporated into the PCST/BDAS algorithm. The results would be improved detection of thinner as well as lower clouds, the amount of which has not been addressed.

Many improvements to the PCST/BDAS algorithm are possible. Section 3.2.5 deals with cloud discrimination based on the BDAS pattern alone. Given some a priori knowledge of the atmospheric and oceanic conditions, the absolute magnitude of the BDAS can be incorporated into the cloud detection algorithm. Figures 3.9-3.14 suggest that this method should have some success. One other step that should be taken is to couple the BDAS with the absolute radiometric single channel measurement of the scene. This will surely help classify scenes where difficulties exist using the BDAS alone; for example, thin cirrus vs. altostratus, clear sky vs. fog, etc.

Other techniques can be used with the MISR data. One such technique is the Visible/Near-IR Multispectral Discrimination technique (Chapter 2). Stereo, however, is perhaps a more powerful cloud detection technique using MISR data. The natural stereoscopic capability of MISR allows the stereo algorithm to determine the vertical depth measured from the satellite to the scene. Cloud detection is performed by subtracting ex-

isting Digital Elevation Maps from MISR-stereo elevation maps. Any residue above the stereo elevation retrieval uncertainty can be attributed to clouds. The expected vertical height resolution from MISR stereo using the nadir camera and one other camera is shown in Figure 3.15.

MISR stereo does not work for all scene types. Two examples are horizontally homogeneous and semi-transparent scenes. Thus the use of the PCST and the BDAS techniques becomes important. With the above improvements to the PCST/BDAS technique and the inclusion of the stereo technique, MISR should prove to be an effective cloud detecting instrument for all cloud types. Figure 3.16 depicts a possible MISR cloud detection algorithm.

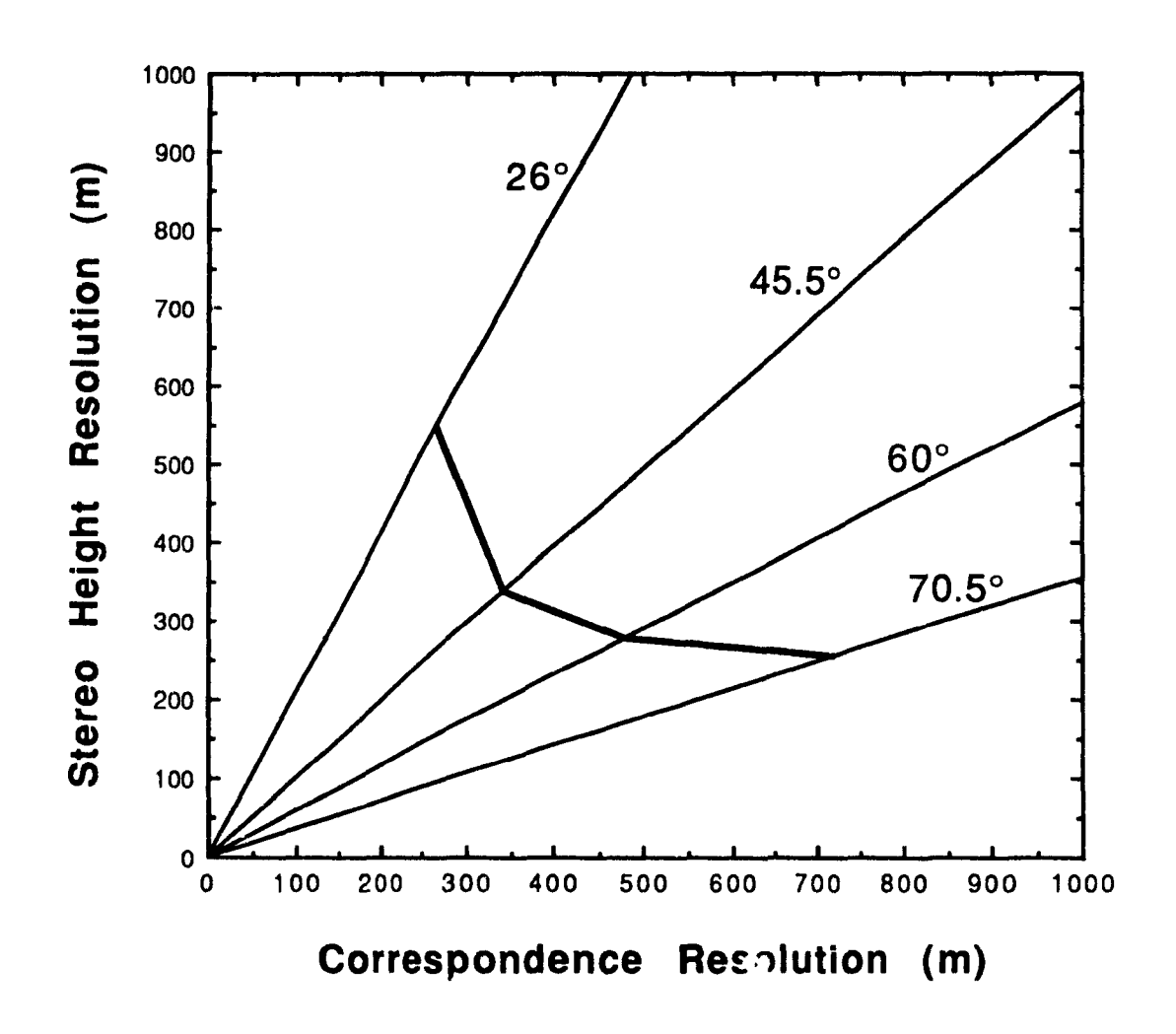


Figure 3.15. Stereo height resolution vs. correspondence resolution for the nadir camera and one other MISR camera (shown here in terms of its surface view angle). The thick joining line represents the MISR single-pixel-level correspondence.

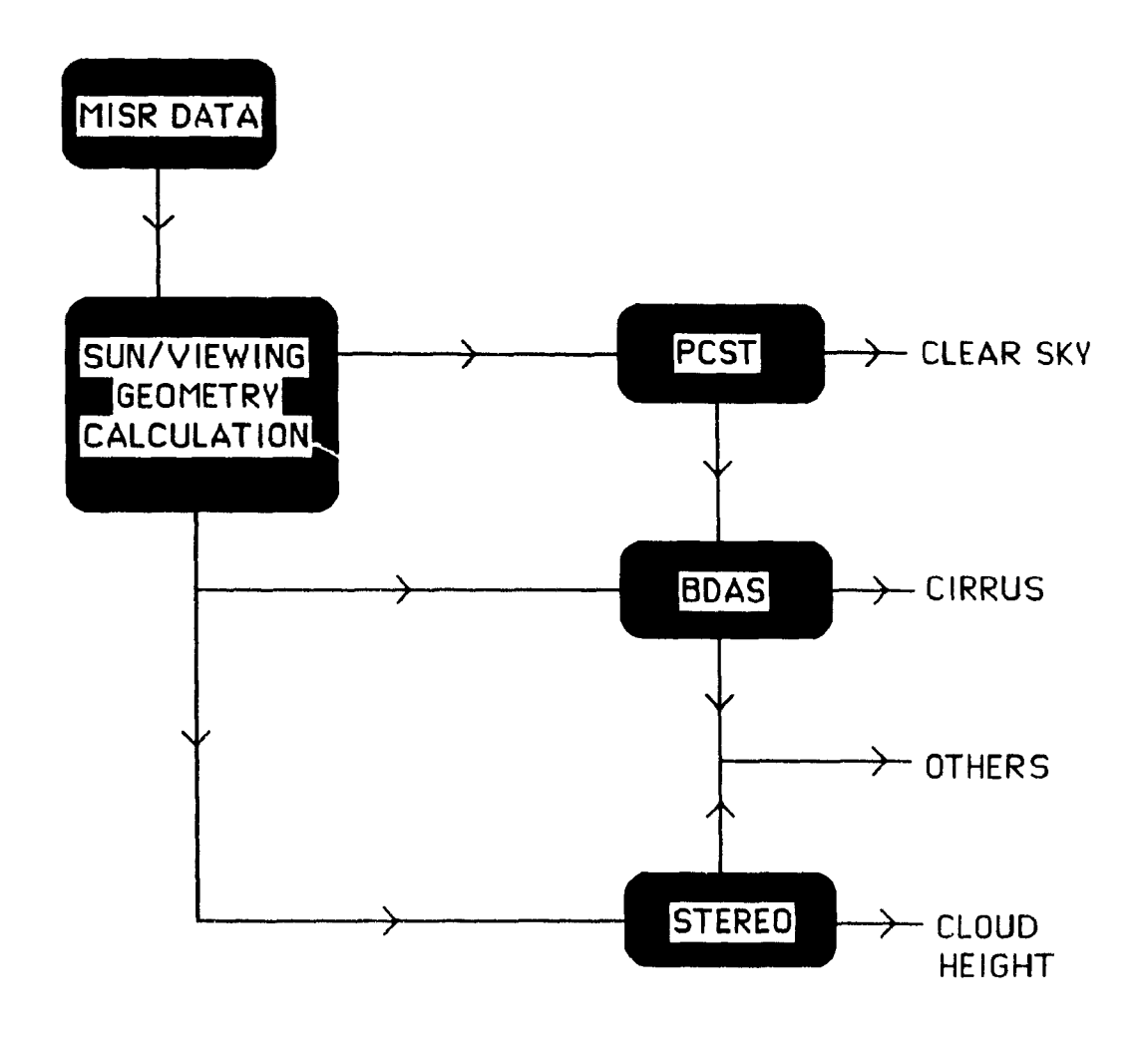


Figure 3.16. The MISR cloud detection algorithm.

## **CHAPTER 4**

## Summary

The role cirrus clouds play on climate feedback remains elusive. This can be attributed principally to the limited amount of information available on all physical quantities which govern the cloud's existence with its environment. Much of our understanding of cirrus clouds has come from computer simulations, especially in the area of radiation-microphysics interactions. However, the complexities involved in modelling the radiative transfer through a medium comprised of non-spherical ice crystals, along with the limited information on other cirrus microphysical properties, has stunted the advancement of our understanding of the bulk radiative effects of cirrus clouds on climate. This has a direct impact on the development of General Circulation Models (GCMs) which require parameterized information of clouds by cloud type. Moreover, GCMs also demand accurate cloud amount climatologies by cloud type, both seasonally and geographically. Thus both microphysical and macrophysical cirrus cloud properties must be obtained with some degree of accuracy if we are to further the development of General Circulation Models.

It has been recognized that the only practical means of obtaining cirrus cloud properties, at many spatial and temporal resolutions, is by satellite remote sensing. This requires algorithms which analyze the information contained in the satellite radiance measurements. Chapter 2 underlined the need for proper detection of cirrus clouds. A review of the performance of existing cloud detection algorithms was made by present-

one cloud algorithm in deriving cloud amount, two important steps were found to be lacking. The first is a cloud definition. Because a precise definition of what constitutes a cloud does not presently exist, the accuracy of a cloud detection algorithm becomes somewhat vague. Secondly, validation must be carried out over sufficient temporal and spatial scales to cover the multitude of scene type scenarios, thus ensuring that the retrieved "accuracy" is not biased toward any particular scene type.

In terms of their relative performance for detecting cirrus clouds, those algorithms which use an IR threshold all perform equally when using the same IR threshold window. Many of the differences between these algorithms can be attributed to the methodology used to determine the thresholds. A significant problem with these algorithms is caused by their inability to detect cirrus clouds having emissivities less than one. This, in effect, lowers the brightness temperature of the cloud which has been calculated under the black cloud assumption. The result is the misclassification of cirrus clouds as low or middle clouds. To escape this problem, algorithms which calculate cloud top pressure (e.g. CO<sub>2</sub> slicing techniques) are preferred for detecting cirrus clouds. Unfortunately, such techniques offer very poor spatial resolutions.

To alleviate the problems of misclassification and poor spatial resolution, a new cloud detection technique has been developed in Chapter 3. This new technique takes advantage of the multi-angle viewing capability of the Multi-angle Imaging SpectroRadiometer (MISR). By combining the spectral and angular information of the radiance emerging from the scene, the Band Differenced Angular Signature (BDAS) is formed. MISR's 0.86

μm reflectance is subtracted from the 0.44 μm reflectance and is plotted as a function of view angle. The resulting BDAS discriminates between cirrus clouds and lower level clouds/fog/clear sky. With the addition of the Predetermined Clear Sky Threshold (PCST), the clear sky scenes are readily identified. Without any a priori knowledge of the atmospheric and oceanic conditions, this new method is capable of detecting cirrus clouds as thin as 0.5 visible optical thickness. If a priori information of the atmospheric and oceanic conditions is known, as required/assumed by most other cloud detection algorithms, then thinner cirrus clouds would most assuredly be detectable.

Keep in mind, however, that the minimum detectable cirrus cloud optical thickness of 0.5 was determined using radiative transfer simulations. Ultimately, the true test can only be done using real data (as opposed to simulated data). Knowing this, the PCST/BDAS algorithm was tested under what was believed to be the worst case scenarios. Since MISR won't be obtaining data until 1998, the real value of the simulations is to prepare the science community for the products expected from MISR and to guide the MISR science to am in reaching its science objectives.

The PCST/BDAS algorithm can be improved upon with the addition of other techniques. One such technique comes naturally from MISR's unique multi-angle viewing capability; this technique is stereo. Its ability lies in detecting thick clouds whose morphology is non-homogeneous (i.e. cumulus-type clouds). The retrieved stereo height resolution from MISR data is expected to be between 50 and 200 m (assuming the expected 1/3-pixel correspondence). Thus, a combination of the variety of

possible cloud detecting techniques using MISR data, along with the data's high spatial resolution, will make the MISR cloud detection algorithm (figure 3.16) an important tool in furthering our understanding of the effects of differing cloud types on our climate system.

## REFERENCES

- Allen, R.C., P.A. Durkee, and C.H. Wash, 1990: Snow/cloud discrimination with multispectral satellite measurements. *J. Appl. Met.* 29(10), 994-1004
- Arakawa, A., 1975: Modelling clouds and cloud processes for use in cloud models. *GARP Publ.* Ser. No. 16, WMO, 183-197
- Arking, A., 1991: The radiative effects of clouds and their impact on climate. Bull. Am. Met. Soc. 72(6), 795-814
- Austin, R.W., 1980: Gulf of Mexico, ocean-color surface-truth measurements. Boundary Layer Met. 18(3), 269-286
- Barton, I.J., 1983: Upper level cloud climatology from an orbiting satellite. J. Atm. Sci. 40, 435-447
- Berlyand, T.G. and L.A. Strokina, 1980a: Zonal cloud distribution on the Earth. *Meteor. Gidrol.* 3, 15-23
- Berlyand, T.G. and L.A. Strokina, 1980b: Global distribution of total cloud amount. *Gidrometeoizdata* (translated by S. Warren), Leningrad, 18pp
- Bosenberg, J., A. Ansmann, S. Elouragin, P.H. Flamant, K.H. Klapphech, H. Linne, C. Loth, L. Menenger, W. Michaelis, P. Moerl, J. Pelon, W. Renger, M. Riebesell, C. Senff, P.-Y. Thro, U. Wandinger and C. Wietkamp, 1990: Measurements with lidar systems during the International Cirrus Experiment 1989. Max-Planck-Institut fur Meteorologie Report No. 60, Hamburg
- Cess, R.D., 1987: Exploratory studies of cloud radiative forcing with a general circulation model. *Tellus* 39A, 460-473
- Cess, R.D., G.L. Potter, J.P. Blanchet, G.J. Boer, A.D. Del Genio, M. Deque, V. Dymnikov, V. Galin, W.L. Gates, S.J. Ghan, J.T. Kiehl, A.A. Lacis, H. Le Treut, Z.-X. Li, X.-Z. Liang, B.J. McAvaney, V.P. Meleshko, J.F.B. Mitchell, J.-J. Morcrette, D.A. Randall, L.Rikus, E. Roeckner, J.F. Royer, U. Schlese, D.A. Sheinin, A. Slingo, A.P. Sokolov, K.E. Taylor, W.M. Washington, R.T. Wetherald, I. Yagai and M.-H. Zhang, 1990: Intercomparison and

- interpretation of climate feedback processes in 19 atmospheric general circulation models. J. Geophys. Res. 95(D10), 16601-16616
- Chahine, M.T., 1975: An analytic transformation for remote sensing of clear-column atmospheric temperature profiles. J. Atm. Sci 32, 1946-1952
- Coakley, J.A. and F.P. Bretherton, 1982: Cloud cover from high resolution scanner data: Detecting and allowing for partially filled fields of view. J. Geophys. Res. 87, 4917-4932
- Coakley, J.A., 1987: A dynamic threshold method for obtaining cloud cover from satellite imagery data. J. Geophy. Rev. 92(D4), 3985-3990
- Cox, S.K., 1971: Cirrus clouds and the climate. J. Atm. Sci 28, 1513-1515
- Cox, S.K., D.S. McDougal, D.A. Randall, and R.A. Schiffer, 1987: The First ISCCP Regional Experiment (FIRE). Bull. Am. Met. Soc. 67, 114-118
- Desbois, M. and G. Seze, 1984: Use of space and time sampling to produce representative satellite cloud classification. Ann. Geophys, 599-606
- Diekmann, F.J. and G.L. Smith, 1989: Investigation of scene identification algorithms for radiation budget measurements. *J. Geophys Res.* \$4, 3395-3412
- Diner, D.J., C.J. Bruegge, J.V. Martonchik, T.P. Ackerman, R. Davies, S.A.W. Gerstl, H.R. Gordon, P.J. Sellers, J. Clark, J.A. Daniels, E.D. Danielson, V.G. Duval, K.P. Klaasen, G.W. Lilienthal, D.I. Nakamonto, R.J. Pagano, and T.H. Reilly, 1989: MISR: A Multiangle Imaging SpectroRadiometer for geophysical and climatological research for EOS. IEEE Trans Geosci. Rem. Sens. GE-27, 200
- Dowling, D.R. and L.F. Radke, 1990: A summary of the physical properties of cirrus clouds. J. Appl. Met. 29, 970-978
- Dozier, J., 1991: Recommended instruments for the restructured Earth Observing System. The Earth Observer 3(6), 1-8

- Ebert, E.E., 1987: A pattern recognition technique for distinguishing surface and cloud types in the polar regions. J. Clim. Appl. Met. 26, 1412-1427
- Ebert, E.E., 1989: Analysis of polar clouds from satellite imagery using pattern recognition and statistical cloud analysis scheme. J. Appl. Met. 28, 382-399
- Eck, T.F. and V.L. Kalb, 1991: Cloud-screening for Africa using geographically and seasonally variable infrared threshold. *Int. J. Remote Sens.* 12(6), 1205-1222
- Eyre, J.R. and W.P. Menzel, 1989: Retrieval of cloud parameters from satellite sounder data: A simulation study. J. Appl. Met. 28, 267-275
- Gallery, W.O., F.X. Kneizys and S.A. Clough, 1983: Air mass computer program for atmospheric transmittance/radiance calculations: FSCATM. AFGL-TR-83-0065
- Goodman, A.H. and A. Henderson-Sellers, 1988: Cloud detection analysis: A review of recent progress. Atm. Res. 21, 203-228
- Goody, R.M., 1964: Atmospheric Radiation, Oxford Press
- Gove, P.G. (editor), 1986: Webster's third new international dictionary, Merriam-Webster Inc.
- Hansen, J., G. Russell, D. Rind, P. Stone, A. Lacis, L. Travis, S. Lebedeff and R. Ruedy, 1983: Efficient three-dimensional global models for climate studies: Models I and II. Mon. Wea. Rev. 11, 609-662
- Henderson-Sellers, A., 1986: Layer cloud amounts for January and July 1979 from 3D-nephanalysis. J. Clim. Appl. Met. 25, 118-132
- Henderson-Sellers, A., G. Seze, F. Drake and M. Desbois, 1987: Surface-observed and satellite-retrieved cloudiness compared for the 1983 ISCCP special study area in Europe. J. Geophys. Res. 92(D4), 4019-4034
- Ilolle, R.L. and S.A. Mackay, 1975: Tropical cloudiness from all-sky cameras on Barbados and adjacent Atlantic Ocean. J. Appl. Met. 14, 1437-1450

i,

- Hughes, N.A. and A. Henderson-Sellers, 1985: Global 3D-nephanalysis of total cloud amount: Climatology for July 1979. J. Clim. Appl. Met. 24, 669-686
- Hwang, P.H., L.L. Stowe, H.Y.M. Yeh and H.L. Kyle, 1988: The Nimbus-7 global cloud climatology. *Bull. Am. Met. Soc.* 69(7), 743-852
- Inoue, T., 1987: A cloud type classification with NOAA 7 split-window measurements. J. Geophys. Rev. 92(D4), 3991-4000
- Isaacs, R.G., W.-C. Wang, R.D. Worsham and S. Goldenberg, 1987: Multiple scattering LOWTRAN and FASCODE models. Appl. Opt. 26(7), 1273-1281
- JPL, 1990: Preliminary experiment implementation plan for the Earth Observing System (EOS) Multi-angle Imaging SpectroRadiometer (MISR). Jet Propulsion Laboratory, California Institute of Technology, Pasadena, CA.
- Kneizys, F.X., E.P. Shettle, L.W.Abreu, J.H. Chetwynd, G.P. Anderson, W.O. Gallery, J.E.A. Selby and S.A. Clough, 1988: Users guide to LOWTRAN 7. AFGL-TR-88-0177
- Kneizys, F.X., E.P. Shettle, W.O. Gallery, J.H. Chetwynd, L.W. Abreu, J.E.A. Selby, S.A. Clough and R.W. Fenn, 1983: Atmospheric transmittance/radiance: computer code LOWTRAN 6. AFGL-TR-83-0187
- Kneizys, F.X., E.P. Shettle, W.O. Gallery, J.H. Chetwynd,
  L.W.Abreu, J.E.A. Selby, R.W. Fenn and R.A. McClatchey, 1980:
  Atmospheric transmittance/radiance: computer code LOWTRAN 5.
  AFGL-TR-80-0067
- Lindner, B.L. and R.G. Isaacs, 1990: Multispectral cloud property retrieval. Am. Met. Soc. -7th Conf. Atm. Rad, July 23-27, 312-319
- Liou, K.N., 1986: Influence of cirrus clouds on weather and climate processes: A global perspective. Mon. Wea. Rev. 114, 1167-1199
- Liu, G.-R., W.L. Smith and T.H. Achtor, 1988: The use of visible data in VAS temperature soundings. J. Appl. Met. 27, 1309-1321
- London, J., 1957: A study of the atmospheric heat balance. Final Report AFC-TR-57-287, OTSB129551, Coll. of Eng. N.Y.U., 99pp.

- Lovejoy, S., D. Schertzer and A.A. Tsonis, 1987: Functional box counting and multiple elliptical dimensions in rain. *Science* 235, 1036-1038
- Malick, J.D., J.H. Allen and S. Zakanycz, 1979: Calibrated analytical modelling of cloud-free intervals. *Proc. Soc. Photo-Opt. Instrum. Eng.* 195, 142-147
- Manabe, S. and R.T. Wetherald, 1967: Thermal equilibrium of the atmosphere with a given distribution of relative humidity. J. Atm. Sci. 24, 241-259
- McGuffie, K. and A. Henderson-Sellers, 1989: Almost a century of "imaging" clouds over the whole-sky dome. *Bull. Am. Met. Soc.* 70(10), 1243-1253
- Merritt, E.S., 1966: On the reliability and representativeness of sky cover observation. J. Appl. Met. 5, 369
- Minnis, P., E.F. Harrison and G.G. Gibson, 1987: Cloud cover over the equatorial eastern pacific derived from July 1983 International Satellite Cloud Climatology Project data using a Hybrid Bispectral Threshold method. J. Geophys. Rev. 92(D4), 4051-4074
- Minnis, P. and B.A. Wielicki, 1988: Comparison of cloud amounts derived using GOES and Landsat data. J. Geophys. Res. D93, 9385-9403
- NASA, 1991: EOS reference handbook. NASA Goddard Space Flight Center, Greenbelt, MD
- NASA, 1976: U.S. Standard Atmospheric Supplements, 1976, U.S. Government Printing Office, Washington, D.C.
- NASA, 1966: U.S. Standard Atmospheric Supplements, 1966, U.S. Government Printing Office, Washington, D.C.
- Parker, L. and B.A. Wielicki, 1989: Comparison of satellite based cloud retrieval methods for cirrus and stratocumulus. NASA CP-3079, FIRE Science Results 1989, 263-270
- Payne, R.E., 1972: Albedo of the sea surface. J. Atmos. Sci. 29, 959-970
- Platt, C.M.R., D.W. Reynolds, and N.L. Abshire, 1980: Satellite and lidar observations of the albedo, emittance and optical depth of

- cirrus compared to model calculations. Mon. Wea. Rev. 108, 195-204
- Prabhakara, C., R.S. Fraser, G. Dalu, M.L.C. Wu, R.J. Curran and T. Styles, 1988: Thin cirrus clouds, seasonal distribution over oceans deduced from Nimbus-4 IRIS. J. Appl. Met. 27, 379-399
- Preisendorfer, R.W. and C.D. Mobley, 1986: Albedos and glitter patterns of a wind-roughened sea surface. J. Phys. Oceanogr. 16, 1293-1316
- Ramanathan, V., R.D. Cess, E.F. Harrison, P. Minnis, B.R. Backstrom, E. Ahmad, and D. Hartmann, 1989: Cloud-radiative forcing and climate: results from the Earth Radiation Budget Experiment. Science 243, 57-63
- Ramanathan, V. and W. Collins, 1991: Thermodynamic regulation of ocean warming by cirrus clouds deduced from observations of the 1987 El Niño. *Nature*, *Lond.* 351(6321), 27-32
- Rascke, E., D. Hennings, R. Sefzig and M. Quante, 1989; ICE International Cirrus Experiment, 1989, field phase plan. Institut fur Geophysik und Meteorologie, Koln
- Robinson, D.A., G. Scharfen, M.R. Serreze, G. Kukla and R.G. Barry, 1986: Snowmelt and surface albedo in the Arctic Basin. *Geophys. Res. Lett.* 13, 945-948
- Rossow, W.B., F. Mosher, E. Kinsella, A. Arking, M. Desbois, E. Harrison, P. Minnis, E. Ruprecht, G. Seze, C. Simmer, and E. Smith, 1985: ISCCP cloud algorithm intercomparison. J. Clim. Appl. Met. 24, 877-903
- Rossow, W.B., 1989: Measuring cloud properties from space: A review. J. Clim. 2, 201-213
- Rossow, W.B., L.C. Gardner and A.A. Lacis, 1989: Global, seasonal cloud variations from satellite radiance measurements. Part I: Sensitivity of analysis. J. Clim. 2, 419-458
- Rossow, W.B. and A.A. Lacis, 1990: Global, seasonal cloud variations from satellite radiance measurements. Part I: cloud properties and radiative effects. J. Clim. 3 (11), 1204-1253
- Rossow, W.B. and R.A. Schiffer, 1991: ISCCP cloud data products.

  Bull. Am. Met. Soc. 72(1), 2-20

Sakellariou, N.K. and H.G. Leighton, 1988: Identification of cloud-free pixels in inhomogeneous surfaces from AVHRR radiances. J. Geophys. Res. 93(D5), 5287-5293

,

- Sathyendranath, S. and A. Morel, 1983: Light emerging from the seainterpretation and uses in remote sensing. in *Remote Sensing* Applications in Marine Science and Technology, NATO ASI Series, edited by A.P. Cracknell, 323-357
- Saunders, R.W. and R.T. Kriebel, 1988: An improved method for detecting clear sky and cloudy radiances from AVHRR data. *Int. J. Remote Sens.* 9, 123-150
- Schiffer, R.A. and W.B. Rossow, 1983: The International Saterlite Cloud Climatology Project (ISCCP): the first project of the World Climate Research Program. *Bull. Am. Met. Soc.* 64, 779-784
- Seze, G. and M. Desbois, 1987: Cloud cover analysis from satellite imagery using spatial and temporal characteristics of the data. J. Clim. Appl. Met. 26, 287-303
- Shettle, E.P., F.X. Kneizys, S.A. Clough, G.P. Anderson, L.W.Abreu and J.H. Chetwynd, 1988: Cloud models in LOWTRAN and FASCODE. *CIDOS-88*, October 18-20 workshop, Silver Springs, MD
- Simpson, J.J. and C. Humphrey, 1990: An automated cloud screening algorithm for daytime Advanced Very High Resolution Radiometer imagery. J. Geophy. Res. 95, 13459-13481
- Smith, G.L., R.N. Green, E. Raschke, L.M. Avis, J.T. Suttles, B.A. Wielicki and R. Davies, 1986: Inversion methods for satellite studies of the Earth's radiation budget: Development of algorithms for the ERBE mission. Rev. Geophys. 24, 207-241
- Smith, W.L. and H.M. Woolf, 1976: The use of eigenvectors of statistical covariance matrices for interpreting satellite sounding radiometer observations. J. Atm. Sci. 33, 1127-1140
- Smith, W.L., H.E. Reveromb, H.B. Howell and M.-X. Lin, 1988: Multispectral window radiance observations of cirrus from satellite and aircraft - November 2, 1986 "Project FIRE". NASA CP-3083, FIRE Science Results 1988, 89-93

- Stephens, G.L., S.-C. Tsay, P.W. Stackhouse, and P.J. Flatau, 1990: The relevance of the microphysical and radiative properties of cirrus clouds to climate and climatic feedback. J. Atm. Sci. 47, 1742-1753
- Stowe, L.L., 1984: Evaluation of Nimbus-7 THIR/CLE and Air Force 3D-nephanalysis estimates of cloud amount. J. Geophys. Res. 89, 5370-5380
- Stowe, L.L., C.G. Wellemeyer, T.F. Eck and H.Y.M. Yeh, 1988: Nimbus-7 global cloud climatology. Part I: Algorithm and validation. J. Clim. 1, 445-470
- Stowe, L.L., C.G. Wellemeyer, T.F. Eck and H.Y.M. Yeh, 1989: Nimbus-7 global cloud climatology. Part II. J. Clim. 2, 641-655
- Susskind, J., J. Rosenfield, and D. Reuter, 1984: Remote sensing of weather and climate parameters from HIRS2/MSU on TIROS-N. J. Geophys. Rev. 89, 4677-4697
- Susskind, J., D. Reuter and M.T. Chahine, 1987: Cloud fields retrieved from analysis of HIRS/MSU sounding data. J. Geophys. Rev 92(D4), 4035-4050
- Takano, Y. and K.N. Liou, 1989 (a): Solar radiative transfer in cirrus clouds. Part I: Single-scattering and optical properties of hexagonal ice crystals. J. Atmos. Sci. 46, 3-19
- Takano, Y. and K.N. Liou, 1989 (b): Solar radiative transfer in cirrus clouds. Part II: Theory and computation of multiple scattering in an anisotropic medium. J. Atmos. Sci. 46, 20-36
- Taylor, V.R. and L.L. Stowe, 1984: Reflectance characteristics of uniform earth and cloud surfaces derived from NIMBUS-7 ERB. J. Geophys. Rev. 89, 4987-4996
- Warren, S.G., C.J. Hahn, J. London, R.M. Chervin and R.L. Jenne, 1988: Global distribution of total cloud cover and cloud type amounts over ocean. NCAR-TN-317+STR
- Whitlock, C.H., L.R. Poole, S.R. LeCroy, W.B. Rossow, K.L. Bell, D.A. Robinson and C. Grund, 1989: Comparison of surface-derived and ISCCP cloud optical properties. NASA CP-3079, FIRE Science Results 1989, 351-356
- Wielicki, B.A. and J.A. Coakley, 1981: Cloud retrieval using infrared sounder data: Error analysis. J. Appl. Met. 20, 157-169

- Wielicki, B.A. and R.M. Welch, 1986: Cumulus cloud properties derived using Landsat satellite data. J. Clim. Appl. Met. 25, 261-276
- Wielicki, B.A. and R.N. Green, 1989: Cloud identification for ERBE radiative flux retrieval. J. Appl. Met. 28, 1133-1146
- WMO, 1971: Climate change. WMO-No.195.TP.100, Technical Note No. 79
- Woodbury, G.E. and M.P. McCormick, 1986: Zonal and geographical distributions of circus clouds determined from SAGE data. J. Geophys. Res. 91(D2), 2775-2785
- Wu, M.L.C., 1987: A method for remote sensing the emissivity, fractional cloud cover, and cloud top temperature of high level, thin cirrus. J. Clim. Appl. Met. 26, 225-233
- Yamanouchi, T., K. Suzuki and S. Kawaguchi, 1987: Detection of clouds in Antarctica from infrared multispectral data of AVHRR. J. Met. Jpn. 65, 949-962